Liquid Crystalline Polymer Brushes

by

Kiana Amini

A thesis
presented to the University of Waterloo
in fulfillment of the
thesis requirement for the degree of
Master of Applied Science
in
Chemical Engineering

Waterloo, Ontario, Canada, 2016

I hereby declare that I am the sole author of this thesis. This is a true copy of the thesis, including any required final revisions, as accepted by my examiners.

I understand that my thesis may be made electronically available to the public.

Abstract

Liquid crystalline polymers are one of the best examples of successful interaction between sciences. This interdisciplinary area of study has benefited from popularity of polymers and uniqueness of liquid crystals. Liquid crystals are well-known for their applications in designing liquid crystalline displays (LCDs). Polymers, specifically polymer brushes, are attractive due to their ability in surface tailoring. The use of liquid crystalline polymer (LCP) brushes is of interest since they can lead to novel and enhanced methods for surface modification. One example of the potential application of LCP brushes is in designing alignment layers for LCDs. In order to design devices based on the LCP brush, it is necessary to understand the physical structure and behaviour of this system under different conditions. To accomplish such understanding, computational and theoretical study of the system can provide advantageous insights.

This project uses the self-consistent field theory to investigate the phase behaviour of liquid-crystalline polymeric brushes immersed in solvent. The polymers are modelled as freely-jointed chain consisting of N rigid segments. The isotropic interactions between the polymer and the solvent are treated using the standard Flory-Huggins theory, while the anisotropic liquid-crystalline (LC) interactions between rigid segments are taken into account using the Maier-Saupe theory.

For weak LC interactions, the brush exhibits the conventional parabolic-like profile, called conventional brush (CB), while for strong LC interactions, the polymers order near the substrate into a dense brush, which is called liquid crystalline (LC) brush. Free energy associated with each structure is calculated and the stable solutions are identified. It is shown that there is a first-order transition between the CB and LC phase. A phase diagram is created to show the effect of different system variables on the phase behaviour.

Acknowledgements

I would like to express my sincere gratitude to my supervisors, Professor Mark Matsen and Professor Nasser Mohieddin Abukhdeir for their continuous support and guidance throughout my course of studies.

I would also like to thank Dr. Bart Vorselaars for his insightful comments at early stage of this project. A special thanks goes to Dr. Russell Spencer for his help, encouragement and patient responses to my numerous questions.

My deepest gratitude and love belong to Bijan, whose love and support were always with me.

Last but not least, my special thanks goes to my parents and my kind brother for their unconditional love, support and encouragement, without which I would not have come this far.

Dedication

To my beloved parents

Table of Contents

List of Figures

Nomenclature

$\bar{\rho_p}$	Polymer volume fraction
$\bar{\rho_s}$	Solvent volume fraction
χ	Flory-Huggins interaction parameter
χ_{pp}	Flory-Huggins polymer-polymer interaction parameter
χ_{ps}	Flory-Huggins polymer-solvent interaction parameter
χ_{ss}	Flory-Huggins solvent-solvent interaction parameter
ΔF	Difference between isotropic and nematic free energies
δ	Dirac delta function
ϵ	Anisotropic coupling parameter
γ	Angle between the long axis of two rigid rods
$\hat{n}$	Director
λ	Relaxation parameter
ν	Excluded volume
Ω	Solid angle
ϕ	Azimuthal angle
ρ	Concentration
ρ_0	Polymer segment concentration in pure melt

ρ_{end}	End-segment distribution
ρ_p	Polymer concentration
ρ_{sm}	Smeared concentration
ρ_s	Solvent concentration
σ	Grafting density
θ	Angle between the long axis of the molecule and the director
ξ	Pressure field
ξ_{pp}	polymer-polymer pair interaction parameter
ξ_{ps}	polymer-solvent pair interaction parameter
ξ_{ss}	solvent-solvent pair interaction parameter
a	Length of each rigid rod
B	Second virial coefficient
b	Effective potential
d	Diameter
E	Total energy
F	Helmholtz free energy
$f(\theta, \phi)$	Orientational distribution function
F_{01}	Free energy of the isotropic phase
F_1	Free energy of the nematic phase
k	Iteration step
k_B	Boltzmann constant
L	Polymer brush height in strong-stretching theory
L_b	Length of the system box

N	Number of the rigid rods
n	Total number of the polymer and solvent molecules
n_h	Number of histories in Anderson-mixing method
n_p	Number of the polymer molecules
n_r	Maximum number of histories in Anderson-mixing method
n_s	Number of the solvent molecules
P	Probability
P_n	n^{th} degree Legendre polynomial
Q	Partition function
q	Forward propagator
$q^\dagger$	Backward propagator
Q_s	Solvent partition function
S	Entropy of mixing
S_2	Scalar order parameter
T	Absolute temperature
T_{NI}	Nematic-isotropic transition temperature
U	Average potential
V	Volume
W	Ensemble-average field for isotropic molecular interactions
w	Dimensionless form of the ensemble-average isotropic molecular field
W_{LC}	Ensemble-average field for anisotropic molecular interactions
w_{LC}	Dimensionless form of the ensemble-average anisotropic molecular field
w_{sst}	SST ensemble-average field

z'	Coordination number
z_0	Position of the free end of the polymer chain
$\mathbf{R}$	End-to-end vector
$\mathbf{r}$	Position vector
$\mathbf{u}$	Vector representing the orientation of the molecules
σ'	Standard deviation

Chapter 1

Introduction

1.1 Motivation

One of the most important materials, with respect to our quality of life, are polymers. They are used pervasively in biological and technological applications in different forms such as plastics, rubbers and foams. While most applications of polymers involve bulk materials, modification of the properties of a surface using polymers is another important application. Polymers grafted to a surface, called "polymer brushes", have a wide range of applications as surface modifiers including friction reduction, stabilization of solid/fluid dispersions and corrosion prevention.

Polymer brushes produce surfaces with desirable properties since they can control the interaction of the surface with its surroundings. Popularity of polymer brushes in surface tailoring is also due to their relative ease of preparation. Chemical adsorption of polymer chains to the substrate produces a stable system in different environments. Moreover, grafting can occur to wide variety of polymeric, organic and inorganic substrates such as nylon, cellulose and gold.

The properties of the grafting surface can be tuned by using different brush chemistries. For instance, to obtain a hydrophilic substrate, one can use polyethylene glycol (PEG) brushes. Apart from polymer chemistries, number of the grafted polymers (grafting density) is also important as it controls the access of surrounding molecules to the substrate. Novel structures can also be obtained by using side chain groups or block copolymers instead of grafted homopolymers.

Other types of important materials in today's technological world are liquid crystalline

(LC) compounds. A liquid crystal is a state of matter that shares properties with conventional liquids and crystalline solids. Similar to crystalline solids, the LC phase is anisotropic. Anisotropy means that properties such as optical, thermal and electrical conductivity vary with direction. Additionally, LC molecules possess some physical features of liquids. For instance, molecules in LC phase can flow similar to liquids. These unique properties of LC material have opened up new doors in theoretical and experimental studies.

Numerous examples of liquid crystalline materials exist both in nature and technological applications. Tobacco mosaic virus, cell membrane and many proteins can form a liquid crystalline phase. Liquid crystals are also recognized for their applications in digital displays, thermometers and image processing.

The use of liquid crystalline polymers as brushes is of current interest in that liquid crystalline ordering could both enhance existing surface modification properties and result in the discovery of new ones. One example of a novel application of liquid crystalline polymer (LCP) brushes is their use as alignment layers for liquid crystalline displays (LCDs) [20]. Alignment layers are used in LCDs to impose a specific molecular orientation, which is required for the basic functionality of LCDs. The development of effective and inexpensive alignment layers has been a key challenge in the display industry. The current method that is being widely used to form the proper alignment layers is a mechanical "rubbing" method, which uses a traditional polymer film as an alignment layer. The rubbing technique is a relatively straightforward and inexpensive method [14]. Also, it creates very stable alignment layers and the technique for such a method has been widely investigated and applied in industry. However, there are some difficulties associated with this method.

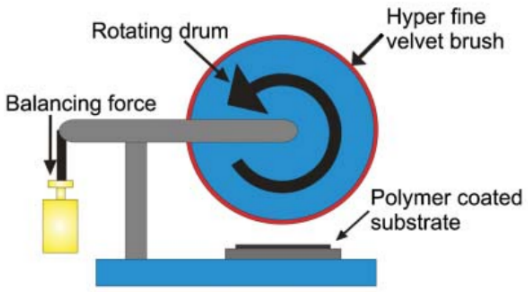

Figure 1.1: Schematic of the rubbing machine. A rotating drum provides a direct contact between the velvet cloth and the spin-coated polymer substrate. This contact forms microscopic grooves on the substrate. Upon interaction with a LC compound, such a substrate induces macroscopic alignment to the neighbouring mesogens. Reprinted from [34].

Electrostatic charges can be generated due to the direct contact of the velvet cloth with the substrate. Additionally, debris of dust might be produced and remain on the substrate. Moreover, it is extremely difficult to create a uniform contrast ratio from site to site on the surface. Due to these problems, faulty pixels are created, which reduces the quality of the production. To minimize these problems, the rubbing process must be done in clean rooms, which makes the procedure highly labour intensive. Furthermore, due to the high demand for larger displays in today's market, it is highly desirable to scale up the process. Thus, bigger substrates are currently desired, which require larger rubber machines. Building such machines would be "a nightmare for engineers to build and operate" [14] .

The previously mentioned issues associated with mechanical rubbing motivates the development of improved methods. Alignment layers composed of LCP brushes are a potential candidate to fill this gap. The formation of LCP brush layers is a "bottom-up" process which is easily scalable to large substrates. Furthermore, polymer brushes are grafted through covalent bonding, which results in increased temperature stability compared to physically deposited polyamide films used in the mechanical rubbing method. The use of LCP brushes also provides various design parameters, such as their molecular weight, grafting density and side chain groups [4], which may be modified to produce the desired properties. In order to properly assess the potential of this approach, detailed theoretical and experimental research is needed.

1.2 Objectives

The overall objectives of this research are:

- To develop a field theoretic model for liquid crystalline polymer brushes immersed in a solvent.
- To find stable configurations of LCP brushes with our model.
- To calculate the degree of orientational order of molecules in these configurations.
- To generate a phase diagram for LCP brushes with different chain lengths, liquid crystallinity and grafting densities.

1.3 Thesis organization

Chapter 2 provides an introduction to polymer brushes and liquid crystals. It will also review recent theoretical progress in studying LCP brush systems. Chapter 3 covers the derivation of our field-theoretic model for an LCP brush system. It also includes a description of theories that are required for this derivation. It begins by introducing different models for characterizing polymer chains, isotropic and anisotropic interactions in a system. These are the freely-jointed chain, Flory-Huggins and Maier-Saupe models, respectively. Following that, a field-theoretic model for a system of polymer brushes (without LC field) is derived. This preliminary model can be validated by using an existing analytical approximation called strong-stretching theory. This theory is also explained in Chapter 3. Following that, the liquid crystallinity is incorporated in the system and the relevant formulas are derived. Chapter 4 demonstrates the numerical procedures that have been employed to solve the necessary equations. Chapter 5 will present and discuss the results of the calculations. Finally, Chapter 6 summarizes the conclusions from this research project and discusses possible future work.

Chapter 2

Background

2.1 Polymer brushes

Polymer brushes are chains of polymers, which are grafted to a substrate by one end with high grafting densities. Grafting density is expressed as the number of the attached chains per unit area of the substrate.

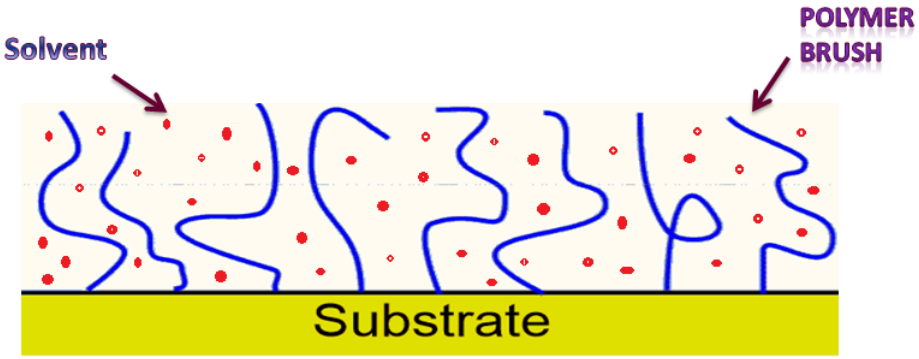

Figure 2.1: A polymeric brush system consists of polymer chains grafted to a substrate at high density. Adapted from [1].

When polymer chains attach to a substrate, according to their grafting density and the strength of the interactions between polymer segments and the substrate, three different conformations of polymer chains can be distinguished [2]:

- For small grafting densities, where the distance between the grafting sites is larger than the size of polymeric chains, the individual chains do not interact with each other and the system behaves similarly to the case of a single grafted chain. In this instance, if weak or repulsive interactions exist between the polymer segments and the substrate, the chains arrange themselves in the shape of a "stem" with different sizes and form a random coil conformation. This kind of structure is called the "mushroom" conformation (Figure 2.2a) [3].

- For small grafting densities and strong attraction between the polymer segments and substrate, chain segments adsorb to the grafting substrate. Thus, the polymer molecules form in a flat shape structure which is called the "pancake" conformation (Figure 2.2b) [3].

- When the grafting density is high, an overlap between polymer molecules occurs. Thus, polymer chains tend to stretch away from the grafting substrate in order to avoid the overlap and minimize the segment-segment interactions. Stretching of the chains reduces the entropy since it diminishes the number of possible chain configurations. Upon reduction of the entropy, retraction forces increase to keep the random-coil configuration in chains. Thus, a new equilibrium is achieved in which grafted polymers are stretched away from the substrate perpendicularly. This conformation which is the focus of this work, is called the "brush" conformation (Figure 2.2c) [3].

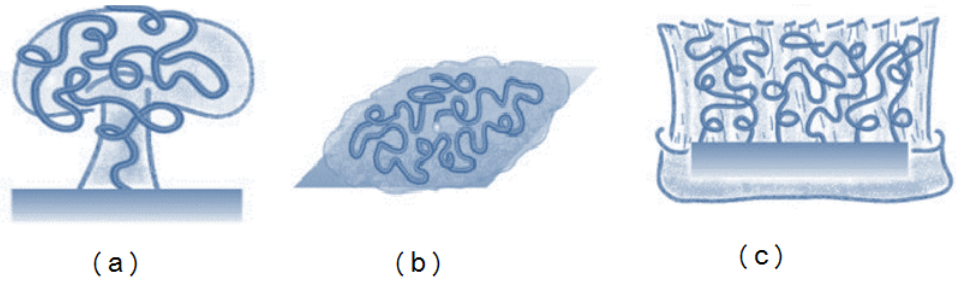

Figure 2.2: Different chain configurations: (a) A mushroom conformation occurs when the grafting density is low and strong repulsion forces exist between grafted chains and the substrate. (b) A pancake conformation occurs when the grafting density is low and strong attraction forces exist between grafted chains and the substrate. (c) A brush conformation occurs when the grafting density is high, which forces the chains to stretch away from the substrate to avoid crowding near the wall. Adapted from [3].

Generally, two different techniques are used to synthesize polymer brushes: physical adsorption (physisorption) and chemical adsorption (chemisorption).

In physisorption, one part of the chain adheres to the surface (van der Waals interactions), while the other part has a repulsive interaction. Thus, the physical adsorption technique is limited to compounds composed of segments with different affinity towards the surface. For instance, it is mostly employed to graft block copolymers to a substrate. As mentioned above, polymer chains adhere to the substrate with weak van der Waal interactions. Thus, a random thermal motion can cause instability in the system. Moreover, this synthesis procedure is reversible. Reversibility of the process and weak van der Waals interactions result in a low grafting density of the produced brush.

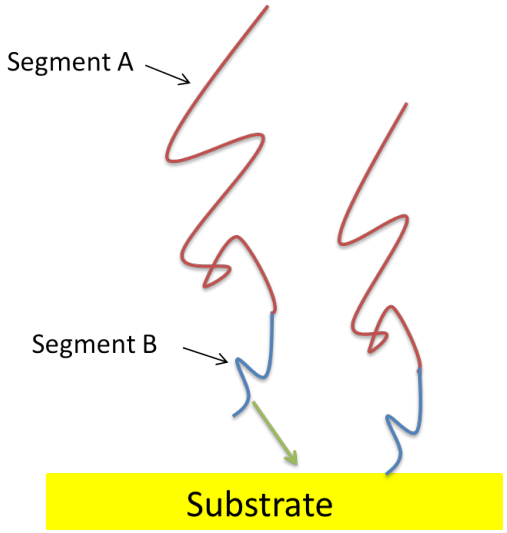

Figure 2.3: Physical adsorption. Block A has low affinity towards the substrate while block B attracts the substrate.

In contrast, chemical adsorption produces polymer chains with more stability towards the environment. This technique produces polymer brushes by creating covalent bonds between polymer ends and the substrate. This covalent bond can be formed with two different procedures: "grafting to" and "grafting from" methods [4]:

- In the "grafting to" approach, a polymer chain with end-functionalized groups is first synthesized from general polymerization techniques. Next, the functionalized end of the polymer chains chemically reacts with compatible reactive groups on the

substrate. In this way, polymers attach to the surface and create brushes. This method has some advantages and disadvantages. The benefit lies in the fact that it is possible to thoroughly characterize the polymers since they are synthesized prior to attachment to the substrate. For instance, one can characterize and control the molecular weight of polymers prior to grafting. A narrow distribution in molecular weight of polymers results in a well-defined system of polymer brushes. However, this method usually produces brushes with low grafting density because the chains must first diffuse through the existing polymeric layer on the substrate to be able to reach the reactive groups.

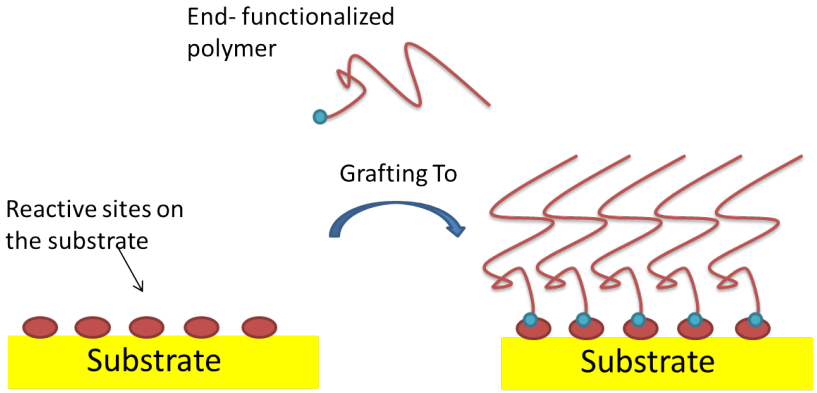

Figure 2.4: "Grafting to" technique. Polymer chains with End-functionalized group are synthesized prior to the grafting and react with active sites on the substrate to form polymer brushes.

- In the "grafting from" approach, first appropriate initiators for the polymerization mechanism are covalently attached to the substrate. Next, by diffusing monomers to the initiators, grafted polymers are generated. Different techniques exist in order to deposit the initiator onto the surface and to perform polymerization. For example, the initiator can be an ion or free radical. The polymerization can be controlled by radical polymerization or ring open polymerization. Thus, by changing the method of initiator deposition, the type of the substrate and the polymerization technique, "grafting from" method can be done in a variety of pathways. Another advantage of this method is that the grafting density of the brush can be controlled since it is possible to increase or decrease the number of the initiator sites on a substrate. As a result, in the "grafting from" method in contrast to the "grafting to" method, one can synthesize a system of polymer brushes with high grafting density by increasing

the number of the initiators [6].

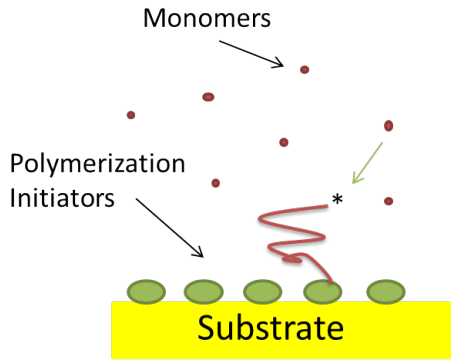

Figure 2.5: "Grafting from" technique. Monomers diffuse to the initiator sites on the substrate to synthesize polymer brushes.

2.2 Liquid crystals

Two familiar types of condensed matter that are abundant in nature are liquids and crystalline solids. Molecules in crystalline solids are positionally and orientationally ordered on a crystalline lattice. In contrast, no positional or orientational order exists in any direction among the molecules in a liquid. Thus, molecules in a liquid are free to diffuse throughout the sample in a random manner. Intermediate to the crystalline solid and liquid is another thermodynamically stable phase (see Figure 2.6). This phase of matter is called liquid crystalline (LC) phase since it shares properties of both liquids and crystalline solids [7]. Molecules in this phase can flow like a liquid but they possess some degree of orientational (and sometimes positional) order. A better understanding of liquid crystalline phases can be achieved by looking at the latent heat of transition. The latent heat of transition from a solid to an LC phase is about 50 times higher than the LC to liquid phase. Therefore, LC phases are more similar to liquids and possess less order than crystalline solids.

Before continuing, it is important to mention some common terms that are used in the liquid crystalline field. Since liquid crystalline phases are intermediate between crystalline solids and isotropic liquids, they are named "mesophases" since "meso" means middle in Latin. As a result, molecules in mesophases are called "mesogens" or "mesogenic" units.

In order to form LC phases, mesogens should possess anisotropic shapes. At the proper condition, the anisotropy in the shape causes molecules to adopt a preferred orientation

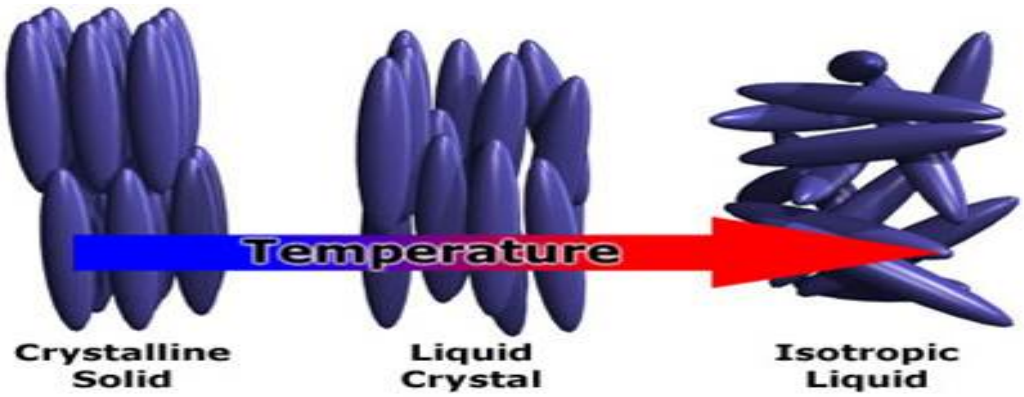

Figure 2.6: Schematic image of molecules in three different phases: the crystalline solid, liquid crystalline and isotropic liquid. Reprinted from [8].

and form an LC phase. Anisotropy often occurs when mesogens contain rigid units (such as a benzene ring or other aromatic rings) and possess flexible tails (e.g. alkane chains). The rigid cores can also be connected with flexible carbohydrate spacers. These elongated structures lead to rod-like shape molecules. Thus, as can be seen in Figure 2.6, mesogens are illustrated as oval objects.

As mentioned earlier, the anisotropy causes the molecules to adopt a preferred direction in an LC phase. By averaging the direction of all the mesogens in the sample, a unit vector is found. This unit vector is called the "director" and is denoted by $\hat{n}$. This director is shown for Figure 2.8.

Liquid crystals are classified into two groups: thermotropic and lyotropic. In thermotropic liquid crystals, the change in temperature is the driving force for phase transition. For instance, the liquid crystalline compound formed by melting a crystalline solid is thermotropic. Thermotropic liquid crystals are currently used in designing LCDs. On the other hand, the phase transition in lyotropic LCs depends on concentration more than temperature. Lyotropic LCs form in mixtures of two (or more) components. Most of the lyotropic compounds are surfactants with one polar and one non-polar end. When such compounds are dissolved at sufficiently high concentration, self-arrangement occurs so that the polar and non-polar ends contact with polar and non-polar solvents, respectively. Thus, an ordered phase is formed. Lyotropic liquid crystals are mostly used as detergents but they also have applications in the oil and food industries.

Liquid crystalline polymers can also be divided into two major classes based on the location of the LC monomers: main-chain LCPs and side-chain LCPs. In the main-chain

LCPs, the mesogenic units are located at the backbone of the polymer (see Figure 2.7a), while in the side-chain LCPs, mesogenic units are connected to the polymer backbone with linking units (see Figure 2.7b).

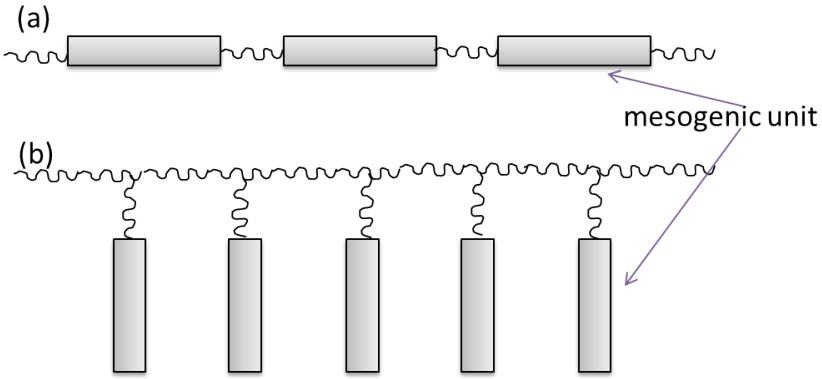

Figure 2.7: Schematic representation of (a) main-chain liquid crystalline polymers and (b) side-chain liquid crystalline polymers. These two groups are identified based on the position of the mesogenic units.

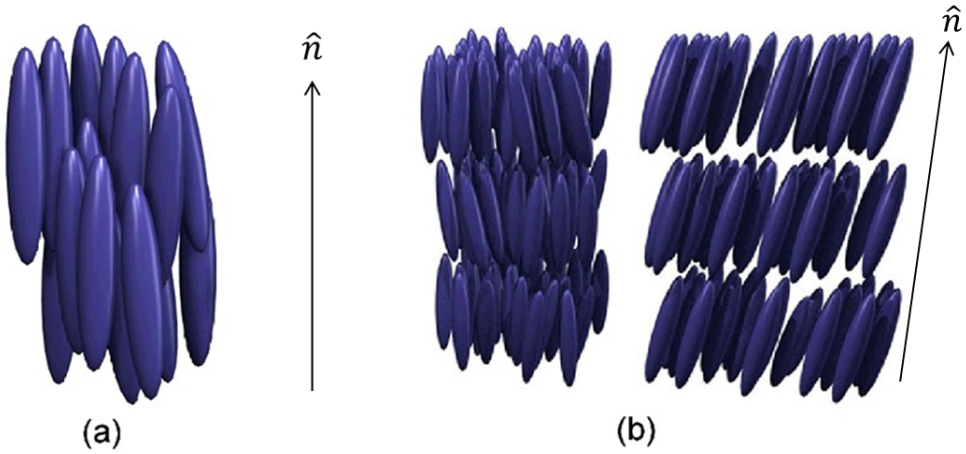

Figure 2.8: Schematic illustrations of (a) nematic LC phase, with a long-range orientational order but no positional order: (b-left) smectic A, where molecules are arranged in layers and oriented perpendicularly with respect to these layers, (b-right) smectic C, where molecules are arranged in layers but are tilted with respect to these layers. $\hat{n}$ is the director. Adapted from [9].

Several types of liquid crystalline phases are identified based on their degree of orientational order. The two most common liquid crystalline phases are nematics and smectics. No positional order exists among molecules in a nematic phase but a long-range orientational order exists in this phase. In a smectic phase, in addition to orientational order, molecules exhibit some positional order where molecules arrange in layers with a well-defined period. Smectics are divided into two categories: smectic A and smectic C. If mesogens are arranged perpendicular to the layers, they are called smectic A liquid crystals. If mesogens make an angle other than 90° with the layers, they constitute a smectic C phase [7]. A schematic of these phases is shown in Figure 2.8.

Order parameter

An important step in defining the liquid crystalline phase is to find a suitable order parameter which quantifies the orientational order of the mesogens. By observing the angular deviation of the long axis of the molecules, $\mathbf{u}$, from the director, the orientational distribution function $f(\theta, \phi)$ can be found [7]. For axially symmetric molecules, the orientational distribution function is only function of the polar angle, θ, and has no dependency on the azimuthal angle, ϕ because in this case, all the orientations perpendicular to the director are equivalent. As a result, we can write $f(\theta, \phi) = f(\theta)$. Note that θ represents the angle that long axis of the molecules make with the director. Next, it is possible to expand $f(\theta)$ in terms of a complete set of orthogonal functions. In orthogonal functions, the product of any two will integrate to give zero (if they are different) or a non-zero value (if they are the same) [10]. Expanding the distribution function in terms of Legendre polynomials (which are orthogonal functions) gives [10]

$$f(\theta) = \sum_{n=0}^{\infty} f_n P_n(\cos\theta) \tag{2.1}$$

where $P_n(x)$ is an n^{th} degree Legendre polynomial. Due to orthogonality, f_n can be expressed as

$$f_n = \frac{2n+1}{2} \int_{-1}^{1} f(\theta) P_n(\cos\theta) d(\cos\theta) = \langle P_n \rangle, \quad n = 0, 1, 2, ... \tag{2.2}$$

Note that if $\mathbf{u} \equiv -\mathbf{u}$, the odd terms in the expansion 2.2 would be zero. Since $f(\theta)$ is known, we can calculate $\langle P_n \rangle$ for every value of n. The most useful one is called the scalar order parameter S_2 and it is defined in terms of the second Legendre polynomial [10]

$$S_2 = \langle P_2(\cos\theta) \rangle = \langle \frac{3\cos^2\theta - 1}{2} \rangle \tag{2.3}$$

In an isotropic phase, where no orientational order exists among the molecules, the probability of occurrence of all the orientations are equal and thus $S_2 = 0$. In a perfectly ordered nematic phase where all the molecules point along the director, $S_2 = 1$. Another ordered system can be achieved if all the molecules orient perpendicular to the director; in that system $S_2 = -1/2$.

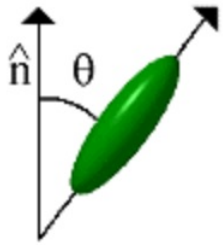

Figure 2.9: θ is the angle that the long axis of molecules makes with the director, $\hat{n}$.

2.3 Previous work

Research on the behaviour of liquid crystalline polymer brushes began with a suggestion from Halperin and Williams in 1993 [15, 16]. Their theoretical work demonstrated the potential of employing liquid crystalline polymer brushes for new applications in the area of smart materials such as designing liquid crystalline displays. These authors considered LCP brushes grafted to a glass substrate and showed that the uncovered portion of the substrate forced the mesogens to orient parallel to the surface (planar alignment) while the LC interactions between the chains resulted in an orientation perpendicular (homeotropic alignment) to the substrate. To determine the outcome of this competition, a mean-field analysis was done and predicted that a tilted alignment would be the product of this competition [4]. Additionally, it is found that the degree of the tilted alignment can be controlled by modifying the grafting density. Since the induction of large tilt angles has been a significant challenge in designing alignment layers, this work motivated further investigation of LCP brushes as alignment layers.

The mentioned studies started a series of theoretical investigations on LCP brushes among other scientists in this field. However, progress in experimental studies has been slower [20]. The experimental studies, in contrast to the system suggested by Halperin and Williams [15, 16], are all focused on side-chain LCP brushes. Two reasons are given for this choice. It has been reported that it is easier to find side-chain LCPs that show good

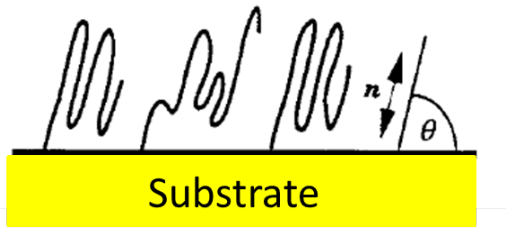

Figure 2.10: Tilted alignment of polymer chains. This arrangement is the product of a competition, in which the crowding of the brush forces the chains to stretch away and form a homeotropic alignment, while the bare substrate induces a planar alignment. The tilt angle θ can be tuned by modifying the grafting density.

miscibility with low molecular weight nematics [4], [32], [33]. Another mentioned reason is that the nematic-to-isotropic transition temperature is lower in most side-chain LCP brushes compared to the main-chain brushes [33]. As mentioned before, the generation of the tilted alignment depends on the competition between the bare substrate and the brush configuration. However, in side-chain LCP brushes, stretching of the main-chains leads to a parallel alignment instead of a perpendicular one because this time the mesogenic units are located in the side chains rather than the backbone of the polymer. Bare substrates also induce parallel alignment as mentioned before. Thus, no competition occurs and the planar alignment is produced. In order to solve this problem, the substrate must be modified beforehand in a way that favours the perpendicular orientation [4], [32].

On the other hand, theoretical studies have focused more on the main-chain LCPs. As mentioned in the section 2.2, liquid crystals are classified into two groups: lyotropic and thermotropic groups. The lyotropic main-chain liquid crystalline polymer brushes have been investigated in [17] using the self-consistent field theory. A worm-like chain model is used and the orientationally-dependant interactions between polymer segments are modelled using the Onsager theory. Onsager theory takes into account the excluded-volume, ν, effect in the system. Thus, system parameters in this model are $\frac{L}{a}$ and $\frac{\nu\sigma}{a}$, where L is the total length, a is the Kuhn length in the worm-like chain model and σ is the grafting density. They found that the brush has a parabolic concentration profile for long chains, $\frac{L}{a} \gg 1$ and low $\frac{\nu\sigma}{a}$, which is similar to the non-LCP brushes found by strong-stretching theory. For $\frac{L}{a} \gg 1$ and high values of $\frac{\nu\sigma}{a}$, the brush has a step-like concentration profile.

As for thermotropic LCPs, the Birshtein group [20] has carried out investigations for more than ten years. This group has used the mean field theory to derive a lattice model

for a system of thermotropic main-chain liquid crystalline polymer brushes immersed in solvent. For these investigations, they considered a layer of flexible chains grafted to a surface with the free ends of the chains on the external boundary of the layer. The Flory-Huggins and Maier-Saupe models are used for isotropic and anisotropic interactions, respectively. The brush is immersed in a solvent and it is assumed that the chains walk on a simple cubic lattice (SCL). A 6-choice SCL model is used, where rigid rods are only allowed to orient in 6 directions ($\pm z$ and 4 directions perpendicular to z) [20]. This assumption, while not realistic, significantly simplifies the model. Additionally, they assumed that mesogens are completely flexible and can easily fold back and forth so that no bending energy is taken into account in their 6-choice SCL model. However, LC polymers are semi-flexible and folding (choosing the back-step) requires energy. In order to improve the model for semi-flexible LC polymers, they investigated the same system with a 5-choice SCL model, where mesogens are prohibited from choosing the back-step, which is not entirely a realistic assumption. Instead of removing the back-step, the bending energy associated with folding should be calculated.

They reported three different configurations for the LCP brush, which are called conventional brush (CB), liquid crystalline (LC) brush and microphase-segregated brush (MSB).

Conventional brushes (CB) form when a weak anisotropic interaction exists between the mesogens. This configuration is similar to the arrangement of segments with only isotropic interactions (no LC segments). Thus, this is a well-known structure that has already been studied thoroughly; in a good solvent, brushes possess a parabolic concentration profile that is also predicted by an analytical approximation called strong stretching theory (Chapter 3). Moreover, calculation of the order parameter for such a system shows that this configuration is highly disordered as expected (Figure 2.13).

LC brushes occur when strong anisotropic interactions exist among mesogens. As evident in Figure 2.11, a step-like dense brush forms near the wall. This structure is highly ordered as can be seen in Figure 2.13. In fact, segments fold back and forth near the wall to maintain a high orientational order. This structure is also called a homeotropic LC (HLC) brush (Figure 2.12).

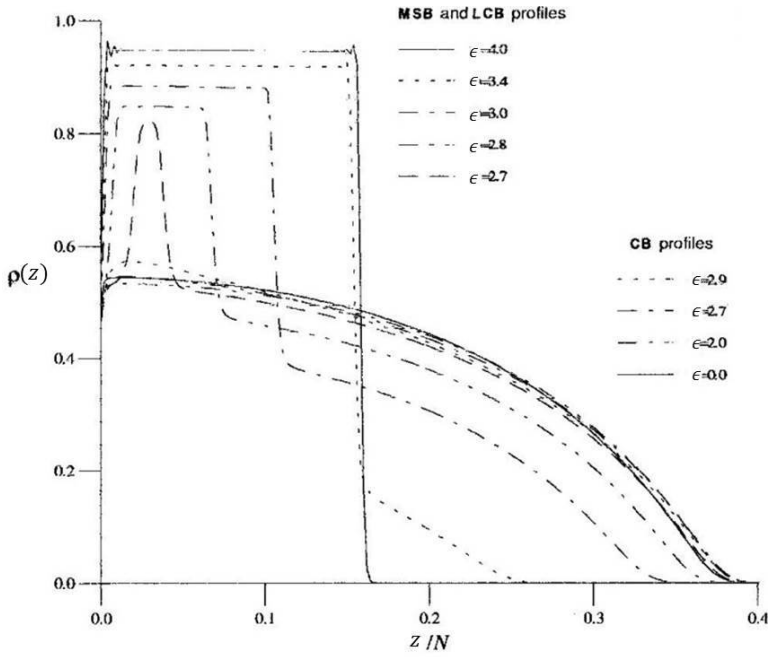

Figure 2.11: Density profile of a single polymer brush for different anisotropic coupling parameters, ϵ: conventional brush (CB) occurs at low ϵ, micro-segregated brush (MSB) forms at intermediate vales of ϵ and liquid crystalline (LC) brush occurs when ϵ is high. N is the number of segments and $\rho(z)$ is the concentration of the segments in the z direction (perpendicular to the substrate). Reprinted from [19].

Figure 2.12: Schematic of homeotropic LC configuration of polymer chains. In a homeotropic LC phase, a dense brush forms near the substrate and polymer chains fold back and forth to maintain a high degree of order.

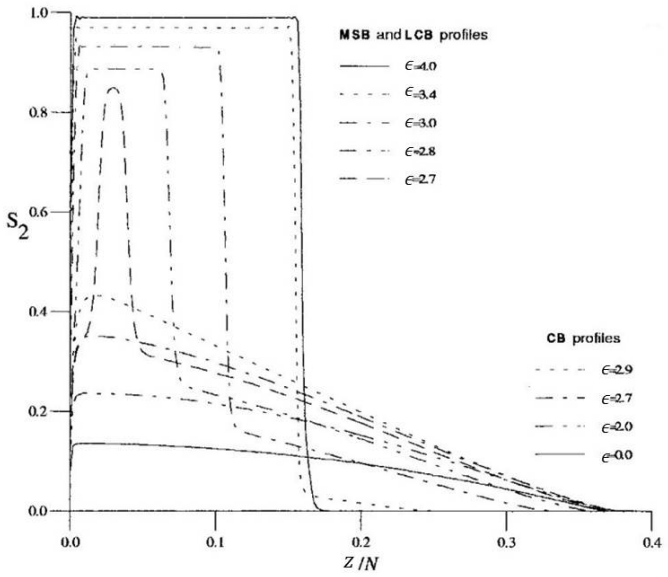

Figure 2.13: Orientational order parameter profile for different phases of polymer brush. Conventional brush (CB), which forms at low ϵ, has a low degree of order, while LC phase is highly ordered with $S_2 = 1$. Order in MSB brush is intermediate between the CB and LC state. Reprinted from [19].

The microphase-segregated brush (MSB) is another configuration that is provided by the Birshtein group. MSB has a combined structure of CB and LC brushes. The internal layer of the brush is collapsed while the external part is swollen [20]. The orientational order profile shows that this structure has some degree of order close to the wall, but it becomes highly disordered far from the substrate (Figure 2.13).

In order to investigate these configurations, the free energy associated with each of the solutions must be calculated. Figure 2.14 is the free energy diagram reported in their work. This diagram shows the dependence of the free energy on the anisotropic coupling parameter, ϵ, (parameter that shows the strength of the LC field and will be discussed in the theory section). In the first region, where the free energy is independent of the anisotropic coupling parameter, the CB configuration forms. In the second region, where the free energy decreases almost linearly with ϵ, the LC brush occurs. These two curves intersect, implying that there is a first-order transition between CB and LC phase (Figure 2.14). It is reported that the MSB structure is found near the transition point.

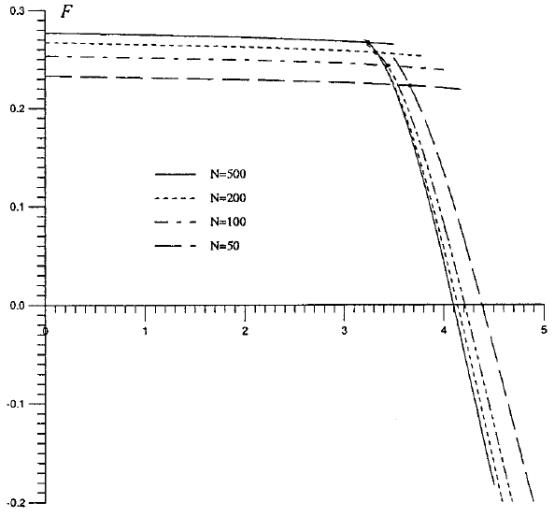

Figure 2.14: Free energy, F, versus anisotropic coupling parameter, ϵ, for chains with different number of segments, N. Here $\sigma = 0.1$, where σ is the grafting density. At low values of ϵ, CB phase is stable and in high ϵ, LC phase is stable. There is a first order transition between these two phases. Increasing the number of chain segments decreases the transition point slightly. Reprinted from [19].

In one of their later works [20], they also mentioned that apart from the homeotropic LC structure (Figure 2.12), a planar liquid crystalline (PLC) structure can form where chains maintain their order by arranging parallel to the wall rather than perpendicularly (Figure 2.15B). However, the free energy diagram showed that the latter conformation is highly unstable (Figure 2.15A). Thus, it can be concluded that two stable solutions exist based on the governing parameters: CB and homeotropic LC.

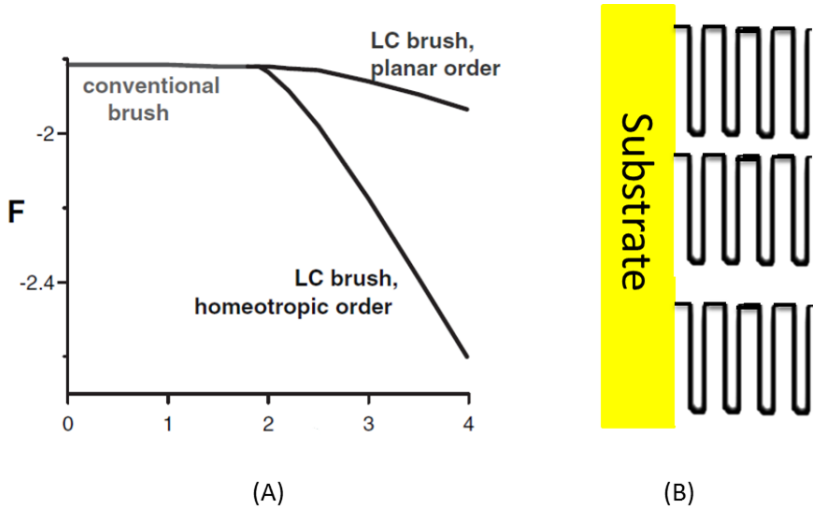

Figure 2.15: (A) The free energy associated with CB, HLC and PLC. The stable phases are conventional brush and homeotropic LC brush. Reprinted from [20]. (B) Schematic illustration of planar liquid crystalline configuration.

All of the calculations in the mentioned work are done for a lattice where the molecules have only 6 choices of angle for their orientation. In order to make the model more realistic, it is important to remove the lattice so that mesogenic units can orient freely.

Chapter 3

Model and theory

This chapter begins by introducing models that are used to represent the liquid crystalline polymer chains and interactions among them. Sections 3.1-3.5 present the freely-jointed chain model, self-consistent field approximation, Flory-Huggins, Maier-Saupe and Onsager model, respectively. In sections 3.6-3.7, a field-theoretic model is derived for a non-liquid crystalline polymer brush. Section 3.8 explains the implicit and explicit solvent methods to incorporate solvent interactions in the system. Section 3.9 employs the implicit solvent method to add solvent interactions in the model. An analytical approximation exists for a system of conventional polymer brushes, which is illustrated in subsection 3.9.1. In section 3.10, the Maier-Saupe model is used to add liquid crystalline interactions to the system. This leads to a model for liquid crystalline polymer brushes immersed in an implicit solvent. A more realistic method to include solvent interactions is the explicit solvent method, which is introduced in section 3.11. Finally, the procedure for the calculation of the free energy for such a system is discussed in subsection 3.11.1.

3.1 Freely-jointed chain model

The freely-jointed chain model is used to describe polymer chains. In this model, polymer chains are modelled as N rigid rods connected to one another with $N+1$ bonds. Each of these bonds is represented by a vector $\mathbf{u}_i = \mathbf{r}_i - \mathbf{r}_{i-1}$ with a fixed length a. This model assumes that there is no restriction in the orientation of the rods and the direction of each bond is independent of the direction of all the other bonds [23]. Since this model assumes that the bond lengths are constant and there is no bending penalty between

successive bonds, it is possible to mathematically formulate the probability distribution of bond vectors as

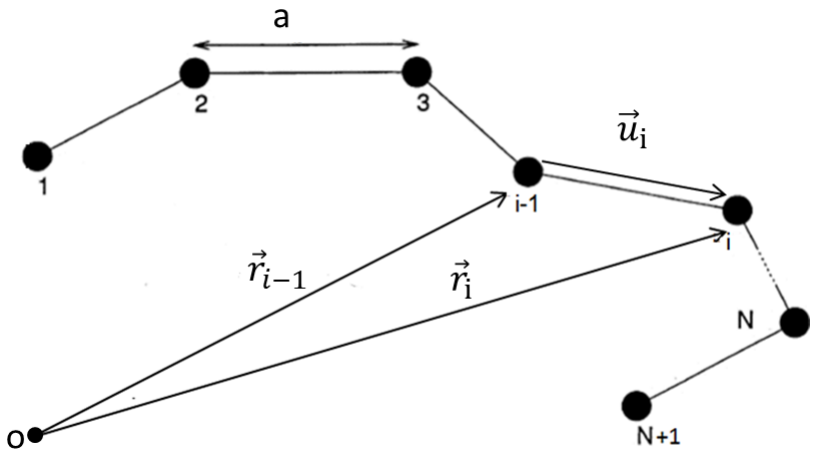

Figure 3.1: Freely-jointed chain model. N rigid rods with fixed length of a are connected with $N+1$ bonds. $\mathbf{r}$ is the position vector and $\mathbf{u}$ is the bond vector.

$$P(\mathbf{u}_i) = \frac{1}{4\pi a^2}\delta(|\mathbf{u}_i| - a) \tag{3.1}$$

where the pre-factor normalizes the probability so that $\int P(\mathbf{u}_i)d\mathbf{u}_i = 1$. Now that the probability distribution of the bond vectors is defined, it is possible to calculate the statistical properties of the freely-jointed chain. In particular, the moments of the end-to-end vector can be calculated. The end-to-end vector, $\mathbf{R} = \mathbf{r}_N - \mathbf{r}_0$, can be expressed as

$$\mathbf{R} = \sum_{j=1}^{N} \mathbf{u}_j \tag{3.2}$$

The first moment

$$\langle \mathbf{R} \rangle = \sum_{j=1}^{N} \langle \mathbf{u}_j \rangle = 0 \tag{3.3}$$

becomes zero since the bonds are isotropically distributed in the space. The second moment is then

$$\langle \mathbf{R}^2 \rangle = \left\langle \sum_{i=1}^{N}\sum_{j=1}^{N} \mathbf{u}_i \cdot \mathbf{u}_j \right\rangle = \sum_{i,j=1}^{N} \langle \mathbf{u}_i \cdot \mathbf{u}_j \rangle \tag{3.4}$$

As mentioned before, each vector is independent of the others and so, terms with $i \neq j$ in the above equation are zero. Thus,

$$\left\langle \mathbf{R}^2 \right\rangle = \sum_{i=1}^{N} \left\langle |\mathbf{u}_i|^2 \right\rangle = Na^2 \tag{3.5}$$

The above equation is equal to $\sqrt{\mathbf{R} \cdot \mathbf{R}} = aN^{\frac{1}{2}}$, which relates the root mean square (RMS) of the end-to-end distance of the polymer chain to the number of segments. Since the freely-jointed chain is an off-lattice model, employing this representation for the chains will produce more realistic results in comparison to the lattice model employed in previous work (mentioned in Chapter 2), which only allowed 6 choices for the orientation of a rod.

In order to investigate this system, we study the interactions of each and every molecule with all the other molecules. However, performing calculations for all the molecules in the system is extremely difficult. To avoid this, the self-consistent field approximation provides an approach to study such a system, which will be discussed in the following section.

3.2 Self-consistent field approximation

In order to investigate a system, it is required to specify the interaction energy of each molecule with all the surrounding molecules. Thus, these calculations are often difficult and computationally expensive. As a result, it is necessary to use some approximations to overcome this barrier. One important class of approximations is called "self-consistent field theory" (SCFT).

This theory uses the concept of an average potential field for an n-particle system. It is assumed that, on average, each molecule undergoes the same forces as any other ones in the system. Thus, it is possible to replace all interactions of any one body with an average or effective interaction called an ensemble-average field, $W(\mathbf{r})$. As a result, instead of doing calculations for all n molecules, this theory simplifies the many-body problem to a one-body problem. The following diagram shows an illustration of applying the mean field approximation to a system of polymer chains [21].

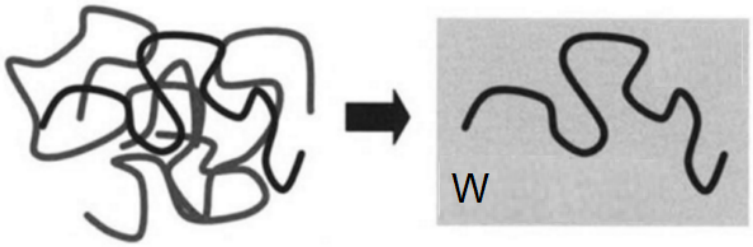

Figure 3.2: Interactions in a many chain system is approximated by introducing an averaged potential field acting on a single chain. Reprinted from [21].

The concept of the mean field approximation is used in the following section to derive an energy for isotropic interactions among the molecules in a system.

3.3 Flory-Huggins model

In order to calculate the energy due to the isotropic interactions between the molecules, we need to discuss the well-known Flory-Huggins model. This is a lattice model that assumes each site on the lattice is occupied either by polymer segments or solvent molecules. For simplicity, this model assumes that a solvent molecule and each segments in a polymer molecule have volumes equal to one site in the lattice. Thus, If we assume n_s is the number of the solvent molecules, n_p is the number of the polymer molecules and N is the number of the segments in the polymer, the total number of sites occupied in the lattice would be $n = n_s + Nn_p$. Equilibrium state in a polymer-solvent mixture is obtained by minimizing the Helmholtz free energy. The Helmholtz free energy is the relevant energy for a system at constant temperature and volume. It is determined by using the total interaction energy E and the sum of the translational and conformational entropy, which is called the entropy of mixing S

$$F = E - TS \tag{3.6}$$

In order to calculate the interaction energy, this theory considers three molecular interactions in the polymer-solvent system [21]: ξ_{ss} is the solvent-solvent pair interaction, ξ_{pp} is the polymer-polymer pair interaction (keep in mind that this is the non-bonded interaction between different chains and not the covalent bonding) and ξ_{ps} is the polymer-solvent pair

interaction. The total interaction energy can be found using the mean-field approximation. Thus,

$$E = \frac{1}{2}\sum_{i}\sum_{\mathbf{a}}\sum_{K=p,s}\sum_{K'=p,s}\xi_{KK'}\rho_K\left(\mathbf{r}_i\right)\rho_{K'}\left(\mathbf{r}_i+\mathbf{a}\right) \tag{3.7}$$

where $\rho(\mathbf{r})$ is the concentration at each position, $\mathbf{r}$ is the position vector shown in Figure 3.1 and $\mathbf{a}$ is a vector pointing to the nearest vectors on the lattice. For the case of a cubic lattice, $\mathbf{a} = (\pm a, 0, 0), (0, \pm a, 0)$ and $(0, 0, \pm a)$, where a is the length of the bonds. If we take z' to be the coordination number of the lattice (6 for a simple cubic lattice), then the above equation reduces to

$$E = \frac{z'n}{2}\sum_{KK'=p,s}\xi_{KK'}\bar{\rho}_K\bar{\rho}_{K'} \tag{3.8}$$

where $\bar{\rho_s}$ and $\bar{\rho_p}$ are obtained by averaging over the position-dependent concentrations (representing the volume fractions of the solvent and polymer in the system).

From the principles of statistical mechanics, one can calculate the entropy change as follow [21]

$$S = -k_B\left(\, n_s\ln\left(\bar{\rho_s}\right) + n_p\ln\left(\bar{\rho_p}\right)\right) \tag{3.9}$$

in which k_B is the Boltzmann constant.

Thus, by substituting equations 3.8 and 3.9 into equation 3.6, we find the free energy of the system

$$\frac{F}{nk_BT} = \sum_{K=p,s} n_K\ln\left(\bar{\rho_K}\right) + \frac{1}{2}\sum_{KK'=p,s}\chi_{KK'}\bar{\rho}_K\bar{\rho}_{K'} \tag{3.10}$$

where $\chi_{KK'}$ is defined as

$$\chi_{KK'} = \frac{z'\xi_{KK'}}{k_BT} \tag{3.11}$$

With this definition, equation 3.8 can be rewritten as

$$\frac{E}{nk_BT} = \frac{1}{2}\left(\chi_{pp}\bar{\rho}_p^2 + \chi_{ss}\bar{\rho}_s^2 + 2\chi_{ps}\bar{\rho}_p\bar{\rho}_s\right) \tag{3.12}$$

In the case of incompressibility, where the total concentration is fixed, we can substitute $\bar{\rho}_s = 1 - \bar{\rho}_p$ in equation 3.12. Thus, the terms containing ${\bar{\rho}_p}^2$ change to

$$-\left(\frac{1}{2}(\chi_{pp}+\chi_{ss}) - \chi_{ps}\right){\bar{\rho}_p}^2 \tag{3.13}$$

The interaction parameters can be grouped into one parameter χ [21]

$$\chi = \frac{1}{2}\left(\chi_{pp} + \chi_{ss}\right) - \chi_{ps} \tag{3.14}$$

where χ is a dimensionless parameter that represents the strength of interactions. It is related to the excluded volume expression as $\nu = \nu_0\left(1 - 2\chi\right)$. When $\chi > \frac{1}{2}$, polymer segments will come together and result in collapsed chains. This type of solvent is called a poor solvent. $\chi = \frac{1}{2}$ is called the theta solvent, in which the effect of the excluded volume is cancelled. When $\chi < \frac{1}{2}$, polymer segments are attracted to solvent molecules and tend to avoid each other. For this case, the solvent is called a good solvent. In the special case of good solvent $\chi = 0$, the solvent is very similar to the monomer which results in similar interactions. This type is called an athermal solvent since temperature has no effect on the resulting structure.

3.4 Maier-Saupe model

Isotropic interactions have no dependency on the orientation of the molecules. However, in the liquid crystalline phase, anisotropy leads to orientational-dependent interactions between LC molecules. Such interactions can be represented using the Maier-Saupe model. The Maier-Saupe model uses the concept of mean field approximation to describe the orientationally dependent interactions between the molecules. The theory starts with three assumptions [7]:

1. The dominant interaction between molecules are van der Waals attraction forces. This theory neglects the effect of excluded volume and repulsive interactions among molecules. Maier and Saupe performed calculations that showed this force is proportional to the inverse sixth power of the distance between the molecules. Thus, as will be shown later, the mean field potential varies as the inverse square of the molecular volume.

2. The second assumption is that symmetry exists along the long axes of the molecules. As a result, there is a dependency on the angle that the long axes of the molecules make with the director.

3. It is assumed that the mean field potential is proportional to the degree of orientational order of molecules. Thus, as will be shown later, S_2 appears in the expression of potential energy as it does.

Based on these assumptions, the Maier-Saupe theory derives a simple expression for the potential energy of a single molecule in the sea of other molecules. In fact, this theory is in the class of self-consistent field theories. The mentioned assumptions lead to the following expression for the average potential [7]

$$U_i\left(\theta_i\right) = -\frac{A}{V^2} S_2 \left(\frac{3\cos^2\theta_i - 1}{2}\right) \tag{3.15}$$

where A is a constant independent of temperature, V is the volume of the sample, S_2 is the order parameter (average of the second Legendre polynomial) and θ, as mentioned before, is the angle that the long axes of the molecules make with the director.

Due to the thermodynamic equilibrium that exists in the system, the probability of a molecule with an orientational angle of θ_i with respect to the director can be found using the Boltzmann weight

$$P_i(\theta_i) = \frac{1}{Q} \exp\left(-\frac{U_i\left(\theta_i\right)}{k_B T}\right) \tag{3.16}$$

where k_B is the Boltzmann constant, T is the absolute temperature of the system and Q is the partition function given by

$$Q = \int_0^{\pi} \exp\left(-\frac{U_i(\theta_i)}{k_B T}\right) \sin\left(\theta_i\right) d\theta_i \int_0^{2\pi} d\phi_i \tag{3.17}$$

where ϕ is the azimuthal angle. Now that we know the probability distribution, we can calculate any average function of θ_i that is desirable. The average of the second Legendre polynomial of $\cos\theta_i$ is of interest since it coincides with the definition of the order parameter

$$\begin{aligned} S_2 = \langle P_2(\cos\theta_i)\rangle &= \left\langle \frac{3\cos^2\theta_i - 1}{2} \right\rangle \\ &= \int_0^{\pi} \left(\frac{3\cos^2\theta_i - 1}{2}\right) P_i(\theta_i) \sin\theta_i d\theta_i \int_0^{2\pi} d\phi_i \end{aligned} \tag{3.18}$$

Thus, we have a self-consistent equation involving the order parameter. Now by averaging over the potential energy shown in equation 3.15, we can find the internal energy, which is

$$\langle U\rangle = E = -\frac{1}{2} c S_2^2 \tag{3.19}$$

where $c = -\frac{A}{V}$ and the coefficient $\frac{1}{2}$ is there to show that the calculations are done in a way that each interaction is counted only once. Based on the Gibbs theory, changes in entropy can be calculated as

$$dS = -k_B P_i \ln(P_i) d\Omega_i \tag{3.20}$$

where $d\Omega_i = \sin\theta_i d\theta_i d\phi_i$. Substitution of equation 3.16 in equation 3.20 would result in

$$S = -k_B \int \left(-\frac{U_i}{k_B T} - \ln(Q) \right) P_i d\Omega_i \tag{3.21}$$

The average energy has been calculated in equation 3.19. Thus, by substituting equation 3.19 in equation 3.21 we obtain

$$S = \frac{-cS_2^2}{T} - k_B \ln Q \tag{3.22}$$

The change in the free energy due to transition from isotropic phase to nematic phase is

$$\Delta F = F_1(S_2 \neq 0) - F_{01}(S_2 = 0) = E - TS \tag{3.23}$$

where F_{01} is the free energy of the isotropic phase and F_1 is the free energy of the nematic phase. By substituting equation 3.19 and 3.22 in equation 3.23, we obtain

$$\Delta F = \frac{cS_2^2}{2} + k_B T \ln Q \tag{3.24}$$

The minimum of ΔF can be found when the order parameter satisfies the consistency condition shown in equation 3.18. By plotting ΔF versus the order parameter, S_2, such a system can be studied. If we denote the temperature of the nematic-isotropic transition as T_{NI}, three cases can be examined:

- For $T < T_{NI}$, the absolute minimum occurs at $S_2 > 0$. This shows that the nematic phase is stable.
- At $T = T_{NI}$, there are two minima. One of the minima is at $S_2 = 0$ and the other is at a positive value of S_2. The free energies of these two states are equal. Thus, at this point a discontinuous transition occurs with an abrupt change in S_2.
- For $T > T_{NI}$ the minimum at $S_2 = 0$ is the absolute minimum, which means that the isotropic phase is stable.

The T_{NI} temperature, at which the free energies of the two minima are equal, is $T_{NI} \approx \frac{c}{4.5415 k_B}$. The order parameter, S_2, corresponding to this temperature is $S_{2,NI} \approx 0.429$ [11]. This value is in close agreement with many reported experiments. Thus, this theory is sufficiently accurate to predict the relationship between the temperature and system properties. As a result, this theory can successfully be used for thermotropic liquid crystalline systems [11].

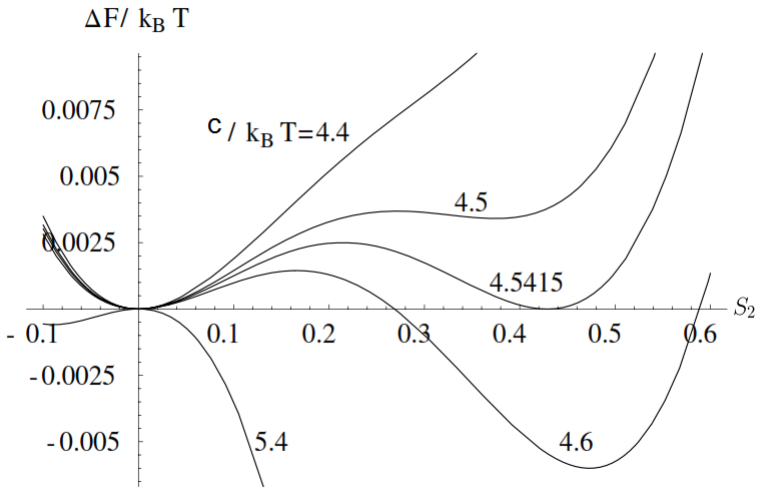

Figure 3.3: Change in the free energy (due to transition from isotropic to anisotropic phase) per molecule versus the scalar order parameter, S_2. Here Different ratios of c/k_BT are shown. $c/k_BT = 4.5415$ shows the case where two minima exist with the same free energy. Thus, it corresponds to $T = T_{NI}$. Examples of $T < T_{NI}$ and $T > T_{NI}$ are also presented. Reprinted from [10].

3.5 Onsager model

As previously mentioned, the Maier-Saupe model assumes that the dominant interactions between the mesogens are the long-range attraction forces. In fact, the Maier-Saupe model neglects the short-range repulsion and the excluded volume effect in the system. Another model exists, which assumes that the short-range repulsive interactions are responsible for the LC ordering. This model, which is called the Onsager model, has the following assumptions [10]:

- The dominant force between the mesogens is the steric effect due to the impenetrability of the mesogens (excluded volume effect).
- Mesogens are cylindrical rigid rods with length a and diameter d where $a \gg d$, which describes an extremely stiff chain.

The basic idea of the Onsager model is that the parallel rods (Figure 3.4) have smaller excluded volume compared to that in the perpendicular arrangement of rods. Thus, the

entropic force of the excluded volume would create an orientationally ordered phase.

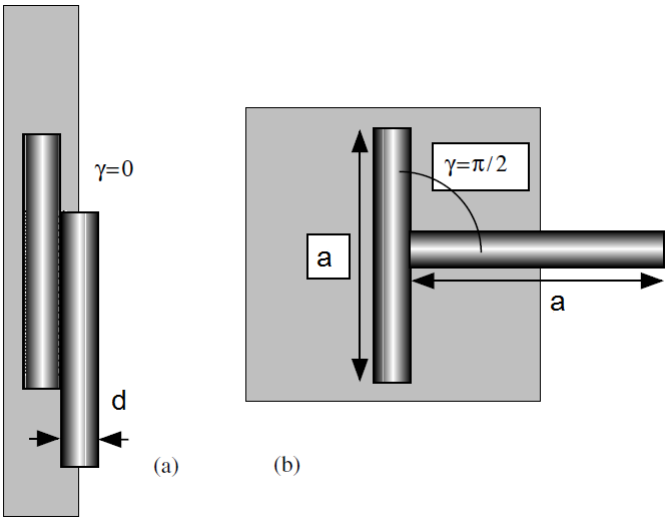

Figure 3.4: Excluded volume effect. d is the diameter, a is the length of the rods and γ is the angle between the long axis of the rods. Parallel rods (Figure a) take a lower volume compared to the perpendicular rods (Figure b). Reprinted from [10].

The Onsager model describes such a system as being made up of N rigid rods in a volume V. Thus, the concentration of such a system is $C = \frac{N}{V}$ and the rods volume fraction is $\bar{\rho} = \frac{\pi C a d^2}{4}$. The orientational distribution function of a rod pointing toward the $\mathbf{u}$ direction with polar angle θ and azimuthal angle ϕ is defined as [10]

$$f(\theta, \phi) d\Omega = f(\mathbf{u}) \sin\theta d\phi d\theta, \tag{3.25}$$

where Ω is the solid angle. With this definition, Onsager introduced the free energy of the system as [12]

$$F = NT[\ln C + \int f(\mathbf{u}) \ln [4\pi f(\mathbf{u})] \, d\Omega_{\mathbf{u}} + \frac{C}{2} \int f(\mathbf{u}_1) f(\mathbf{u}_2) B(\gamma) d\Omega_{\mathbf{u_1}} d\Omega_{\mathbf{u_2}}] \tag{3.26}$$

The free energy due to the translational motion is shown as the first term in equation 3.26. The loss of orientational entropy, which is the result of nematic ordering, is described by the second term. The third term shows the free energy of interactions of a rod pointing toward $\mathbf{u}_1$ direction with a rod of $\mathbf{u}_2$ direction in the second virial expansion. $B(\gamma)$ is the second virial coefficient defined as [12]

$$B(\gamma) = 2L^2 d \sin\gamma \tag{3.27}$$

where γ is the angle between the long axes of the rods. The Onsager model is only accurate for a low concentration of the rods since the second virial approximation is used to include the interactions between the rods.

Now in order to minimize F in equation 3.26, it is necessary to find $f(\mathbf{u})$. The Onsager model employs the variational method with the following trial function [12]

$$f_{\mathbf{u}} = \frac{\alpha}{4\pi \sinh \alpha} \cosh(\alpha \cos\theta) \tag{3.28}$$

where θ is the angle between the long axis of a rod and the director and α is the variational parameter. To find different phases, the trial function is substituted in equation 3.26 and is minimized about α. With this method, Onsager theory showed that the isotropic and nematic transitions occur at the following volume fractions

$$\begin{aligned} \bar{\rho}_{iso} &= 3.34\frac{d}{a} \\ \bar{\rho}_{nem} &= 4.49\frac{d}{a} \end{aligned} \tag{3.29}$$

For $\bar{\rho} < \bar{\rho}_{iso}$, the isotropic phase is stable and for $\bar{\rho} > \bar{\rho}_{nem}$, the nematic phase is stable. For $\bar{\rho}_{iso} < \bar{\rho} < \bar{\rho}_{nem}$, separation into isotropic and anisotropic phases occurs. Additionally, the Onsager theory predicts that the critical degree of orientational order is $S_{2,c} = 0.84$, which is twice the value found by the Maier-Saupe model and experiments.

The Onsager model can describe the behaviour of systems with low concentration (since the second viral approximation is used) having a very high $\frac{a}{d}$, which is usually estimated as $\frac{a}{d} > 10$. For instance, this model accurately predicted the behaviour of a very long polymer with high rigidity called poly(-benzyl L-glutamate) (PBLG) in diaxone water. However, this model is not valid for low-molecular weight nematic systems where usually $\frac{a}{d} \ll 10$. Additionally, no dependency on temperature is included in the Onsager theory. As a result, it cannot be used to describe thermotropic liquid crystals and is limited to lyotropic LCs.

3.6 Polymer in a field

In this project, we are considering a polymer brush, where each polymer consists of a sequence of N rods connected by N bonds. As seen in Figure 3.5, the center of the i^{th} rod (i=1,2,...,N) with respect to the origin is specified by the vector $\mathbf{r}_i = (x_i, y_i, z_i)$ and its orientation is given by the vector $\mathbf{u}_i = (u_{x,i}, u_{y,i}, u_{z,i})$. For simplicity, it is assumed that the length of each rod is uniform, i.e., $a = |\mathbf{u}_i| = 1$. Additionally, the chain end is assumed

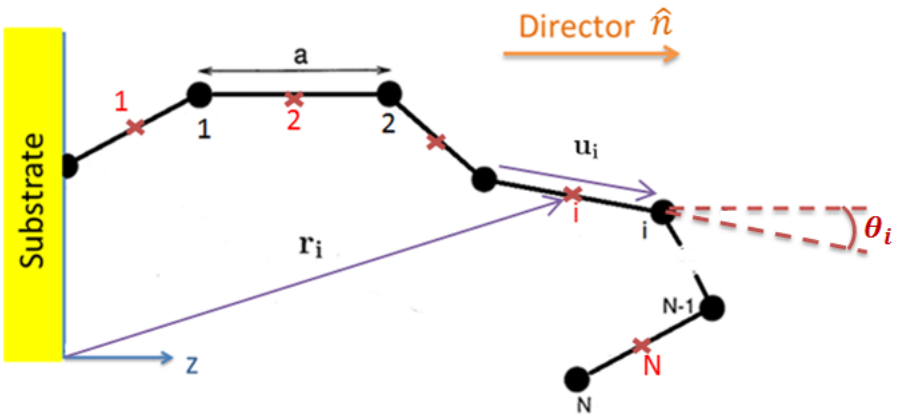

Figure 3.5: Polymer chain with N freely-jointed chains. Positions of the centres of the rods are shown by $\mathbf{r}$ and their orientations are denoted by $\mathbf{u}$. a is the length of the rods. θ is the angle that $\mathbf{u}_i$ makes with the director.

to be grafted at the origin. The angle $\mathbf{u}_i$ makes with the director, $\hat{n}$, is denoted by θ_i. Note that the two bonds of the i^{th} rod occur at $\mathbf{r}_i \pm \frac{1}{2}\mathbf{u}_i$.

Based on the mean-field approximation, an ensemble-average field, $W(\mathbf{r})$, is introduced for intermolecular interactions. For now, only isotropic interactions are considered and no liquid crystalline phase exists in the system. Thus, for this case, the energy of the chain is due to the energy of the bonds between the molecules and the energy resulting from the molecular field.

$$E = \sum_{i=1}^{N} b(\mathbf{u}_i) + \sum_{i=1}^{N} W(\mathbf{r}_i) \tag{3.30}$$

In this equation, the first term is an effective potential that enforces the constraint $|\mathbf{u}_i| = 1$ and the second term is for the field representing the non-bonded molecular interactions (isotropic). With the energy of the chain defined in this manner, we know from statistical mechanics that the probability of a particular configuration of the chain is given by

$$P(\{\mathbf{u}_i\}) = \frac{1}{Q} \exp\left(-E/k_B T\right) \tag{3.31}$$

where Q is the partition function, k_B the Boltzmann constant and T is the absolute temperature. Note that in equation 3.31, the probability of a particular chain configuration is only function of the set $\{\mathbf{u}_i\}$. This is because the system can be defined by knowing $\mathbf{u}_i$ for all the rods since the position vector, $\mathbf{r}_i$ has the following relation with the orientation

vectors (see Figure 3.5)

$$\mathbf{r}_i = \mathbf{u}_1 + \mathbf{u}_2 + \cdots + \mathbf{u}_{i-1} + \frac{\mathbf{u}_i}{2} \tag{3.32}$$

We know that the sum of all the probabilities of different configurations has to be one. Thus, by integrating equation 3.31 with respect to $\mathbf{u}_i$, we obtain 1.0. From this, the partition function must equal

$$Q = \int \exp\left(-E/k_B T\right) \prod_{j=1}^{N} d\mathbf{u}_j \tag{3.33}$$

Now if we hold a rod with $\mathbf{r}_i$ and $\mathbf{u}_i$ at a constant position and orientation and let all the other position and orientation vectors vary, the probability for this is expressed by

$$P_i\left(\mathbf{r}, \mathbf{u}\right) = \int P(\{\mathbf{u}_i\})\delta(\mathbf{r} - \mathbf{r}_i)\delta(\mathbf{u} - \mathbf{u}_i) \prod_{j=1}^{N} d\mathbf{u}_j \tag{3.34}$$

If we substitute equation 3.31 into equation 3.34, we obtain

$$P_i(\mathbf{r}_i, \mathbf{u}_i) = \frac{1}{Q} \int \exp(-E/k_B T)\delta(\mathbf{r} - \mathbf{r}_i)\delta(\mathbf{u} - \mathbf{u}_i) \prod_{j=1}^{N} d\mathbf{u}_j \tag{3.35}$$

Substituting the expression for the energy from 3.30 inside the exponential yields

$$\exp\left(-E/k_B T\right) = \exp\left(-\sum_{i=1}^{N}\left(\frac{b(\mathbf{u}_i) + W(\mathbf{r}_i)}{k_B T}\right)\right) \tag{3.36}$$

Through making use of a mathematical relationship for exponentials, it becomes evident that this expression is just a multiplication of the exponentials

$$\exp\left(-E/k_B T\right) = \prod_{j=1}^{N} \exp\left(-\frac{b(\mathbf{u}_j) + W(\mathbf{r}_j)}{k_B T}\right) \tag{3.37}$$

If we define a new variable

$$g(\mathbf{r}_j, \mathbf{u}_j) = \exp\left(-\frac{b(\mathbf{u}_j) + W(\mathbf{r}_j)}{k_B T}\right) \tag{3.38}$$

The final form of the exponential of the energy becomes

$$\exp(-E/k_BT) = \prod_{j=1}^{N} g(\mathbf{r}_j, \mathbf{u}_j) \tag{3.39}$$

Now for the probability we have

$$P_i(\mathbf{r}_i, \mathbf{u}_i) = \frac{1}{Q} \int \prod_{j=1}^{N} g(\mathbf{r}_j, \mathbf{u}_j) \delta(\mathbf{r} - \mathbf{r}_i) \delta(\mathbf{u} - \mathbf{u}_i) \prod_{j=1}^{N} d\mathbf{u}_j \tag{3.40}$$

In order to simplify the above equations, we define two new parameters called the forward and backward propagators (see Figure 3.6). The forward propagator has the form of

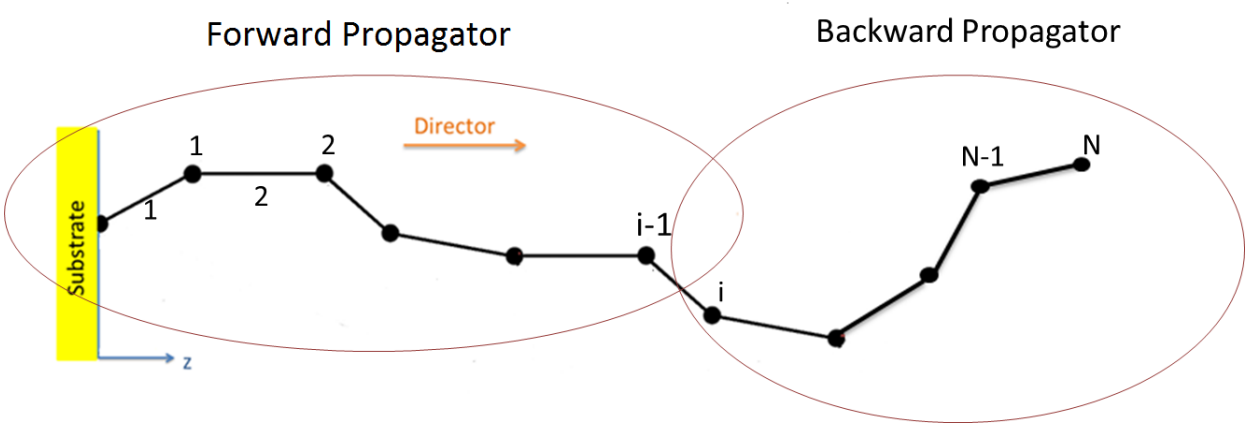

Figure 3.6: Forward and backward propagators

$$q_i(\mathbf{r}) = \int \prod_{j=1}^{i} g(\mathbf{r}_j, \mathbf{u}_j) \prod_{j=1}^{i} d\mathbf{u}_j \tag{3.41}$$

where $\mathbf{r} = \mathbf{r}_i - \frac{1}{2}\mathbf{u}_i$. The backward propagator is

$$q_i^{\dagger}(\mathbf{r}) = \int \prod_{j=i+1}^{N} g(\mathbf{r}_j, \mathbf{u}_j) \prod_{j=i+1}^{N} d\mathbf{u}_j \tag{3.42}$$

where $\mathbf{r} = \mathbf{r}_i + \frac{1}{2}\mathbf{u}_i$. Combination of the forward and the backward propagators will help us to further simplify the calculations of probability density to get

$$P_i(\mathbf{r}_i, \mathbf{u}_i) = \frac{q_{i-1}\left(\mathbf{r}_{i-1} - \frac{\mathbf{u}_{i-1}}{2}\right) q_{N+1-i}^{\dagger}(\mathbf{r}_i + \frac{\mathbf{u}_i}{2}) g\left(\mathbf{r}_i, \mathbf{u}_i\right)}{Q} \tag{3.43}$$

In the following section, we will demonstrate how the equations 3.41 and 3.42 can be modified into convolution integrals to evaluate the propagators.

3.7 Evaluation of propagators

To specify the propagators, we need to start from $i = 1$ for q and $i = N$ for $q^\dagger$ and specify the initial conditions for the two ends. Then, the rest of the points can be evaluated using a convolution integral. The grafted end must satisfy the following initial condition

$$i = 0 : q_0(\mathbf{r}_i) = 2\delta(\mathbf{r}_i)$$

$$i \neq 0 : q_0(\mathbf{r}_i) = 0$$

where δ is the Dirac delta function. The coefficient 2 is used since the Delta function sits on the wall ($\mathbf{r}_0 = 0$) with half of its volume on the positive side. Note that this initial condition for $q_0(\mathbf{r}_0)$ grafts the chain end to the origin ($\mathbf{r}_0 = 0$). Using equation 3.41, we are now ready to calculate the rest of the propagators. We will start with $i = 1$

$$q_1(\mathbf{r}) = \int g\left(\mathbf{r}_1 - \frac{\mathbf{u}_1}{2}, \mathbf{u}_1\right) d\mathbf{u}_1 \tag{3.44}$$

Since the first rod is grafted to the origin ($\mathbf{r}_0 = 0$), we can conclude that $\mathbf{r}_1 = \mathbf{u}_1$. Thus,

$$q_1(\mathbf{r}) = \int g\left(\frac{\mathbf{u}_1}{2}, \mathbf{u}_1\right) d\mathbf{u}_1 \tag{3.45}$$

Applying the same procedure,

$$q_2(\mathbf{r}) = \int g\left(\frac{\mathbf{u}_1}{2}, \mathbf{u}_1\right) g\left(\mathbf{r}_2 - \frac{\mathbf{u}_2}{2}, \mathbf{u}_2\right) d\mathbf{u}_1 d\mathbf{u}_2 \tag{3.46}$$

Note that by looking at equation 3.32, we can see that $\mathbf{r}_2 = \mathbf{u}_1 + \frac{\mathbf{u}_2}{2}$. Thus, the above integral is only over $\mathbf{u}_1$, $\mathbf{u}_2$. For $i = 3$

$$q_3(\mathbf{r}) = \int g\left(\frac{\mathbf{u}_1}{2}, \mathbf{u}_1\right) g\left(\mathbf{r}_2 - \frac{\mathbf{u}_2}{2}, \mathbf{u}_2\right) g\left(\mathbf{r}_3 - \frac{\mathbf{u}_3}{2}, \mathbf{u}_3\right) d\mathbf{u}_1 d\mathbf{u}_2 d\mathbf{u}_3 \tag{3.47}$$

Again, $\mathbf{r}_2 = \mathbf{u}_1 + \mathbf{u}_2 + \frac{\mathbf{u}_3}{2}$ and the above integral is only over $\mathbf{u}_1$, $\mathbf{u}_2$ and $\mathbf{u}_3$. By looking at the above relations for $q_1(\mathbf{r})$, $q_2(\mathbf{r})$ and $q_3(\mathbf{r})$, it is possible to come up with a general formulation for evaluation of propagators

$$q_i(\mathbf{r}) = \int q_{i-1}(\mathbf{r} - \mathbf{u}) g\left(\mathbf{r} - \frac{\mathbf{u}}{2}, \mathbf{u}\right) d\mathbf{u} \tag{3.48}$$

in which the integral is seen to be a convolution. Following the same procedure for $q^\dagger$, we start from the initial condition for the free end

$$i = N : q_N^\dagger(\mathbf{r}_N) = 1$$
$$q_{N+i-1}^\dagger(\mathbf{r}_{N+i-1}) = \int q_{N+i-2}^\dagger\left(\mathbf{r}_{N+i-1} - \mathbf{u}_{N+i-1}\right) g\left(\mathbf{r}_{N+i-1} - \frac{\mathbf{u}_{N+i-1}}{2}, \mathbf{u}_{N+i-1}\right) d\mathbf{u}_{N+i-1} \tag{3.49}$$

These two propagators are only different in their initial conditions because one end is grafted and the other end is free. Other than that, with a little change in numbering the beads, the convolution integral is found to be the same for both propagators. In fact, the backward propagator can be written as

$$q_i^\dagger(\mathbf{r}) = \int q_{i-1}^\dagger(\mathbf{r} - \mathbf{u}) g\left(\mathbf{r} - \frac{\mathbf{u}}{2}, \mathbf{u}\right) d\mathbf{u} \tag{3.50}$$

It is possible to simplify the above equations by positioning the wall with its surface at $z = 0$. In this case, $q(z)$, $q^\dagger(z)$, $g(z, \mathbf{u})$ and $W(z)$ possess translational invariance in the x and y directions. Thus, they are reduced to scalar parameters. Additionally, this invariance allows us to take an integral over u_x ad u_y in equation 3.48 that results in transformation of $g(z, \mathbf{u})$ into

$$g(z, u) \equiv \int g(z, \mathbf{u}) du_x du_y \tag{3.51}$$

where $u = u_z = \cos\theta$. With this, the vectors $\mathbf{u}$ and $\mathbf{r}$ in previous equations reduce into scalars, u and z. Figure 3.7 shows scalars u and z. It is mentioned previously that the length of the rods are assumed to be the same and equal to one ($a = 1$). Thus, $u = \cos\theta$ in which θ is the angle that rods make with the z direction.

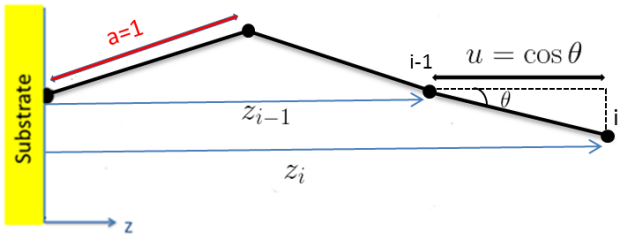

Figure 3.7: Vectors $\mathbf{r}$ and $\mathbf{u}$ reduced to scalars z and u. Since the length of the rods are assumed to be one, it can be concluded that $u = \cos\theta$, where θ is the angle that rods make with the z direction.

Moreover, the recursion relation simplifies to a one-dimensional integral

$$q_i(z) = \int q_{i-1}(z-u)g(z-\frac{u}{2},u)du \tag{3.52}$$

The effective potential for the case of rigid rods is given by

$$\exp\left(-\frac{b(\mathbf{u})}{k_BT}\right) = \frac{1}{4\pi a^2}\delta(|\mathbf{u}|-a) \tag{3.53}$$

and it shows that, for the rigid rods in the freely-jointed chain model, bond lengths are fixed to a constant denoted by a. Additionally, $\frac{1}{4\pi a^2}$ is used to normalize the expression. Using this form for the effective potential, $g(z,\mathbf{u})$ would be

$$g(z,\mathbf{u}) = \frac{1}{4\pi a^2}\delta(|\mathbf{u}|-a)\exp\left(\frac{-W(z)}{k_BT}\right) \tag{3.54}$$

Note that by positioning the wall at $z = 0$, $W(z)$ is translationally invariant. Using equation 3.51, we obtain

$$g(z,u) = \int\int g(z,\mathbf{u})du_xdu_y = \frac{1}{4\pi a^2}\exp\left(\frac{-W(z)}{k_BT}\right)\int\int \delta(|\mathbf{u}|-a)du_xdu_y \tag{3.55}$$

which results in (proof in Appendix A)

$$g(z,u) = \begin{cases} (2a)^{-1}\exp\left(\frac{-W(z)}{k_BT}\right), & \text{if } |u|<a \\ 0, & \text{if } |u|>a \end{cases} \tag{3.56}$$

As mentioned previously, we set $a = 1$. Thus, for $|u| < 1$ we have

$$g(z,u) = \frac{1}{2}\exp\left(\frac{-W(z)}{k_BT}\right) \tag{3.57}$$

We can define a dimensionless field

$$w(z) = \frac{W(z)}{k_BT} \tag{3.58}$$

This would change g to (for $|u| < 1$)

$$g(z,u) = \frac{1}{2}\exp(-w(z)) \tag{3.59}$$

Once we know the propagators and the g function, the probability density of a rod with its center at z and an orientation of $u = \cos\theta$ can be calculated as follows

$$P_i(z,u) = \frac{q_{i-1}\left(z - \frac{u}{2}\right) q^{\dagger}_{N+1-i}\left(z + \frac{u}{2}\right) g(z,u)}{Q} \tag{3.60}$$

where the partition function is

$$Q = \int\int q_{i-1}\left(z - \frac{u}{2}\right) q^{\dagger}_{N+1-i}\left(z + \frac{u}{2}\right) g(z,u) dz du \tag{3.61}$$

It is possible to perform a change of variable on the above equation and generate other formulas for the calculation of the partition function. Obviously, all of such equations would result in the same answers. However, this is a good test to validate our calculation and debug the computer code. If we set $z + \frac{u}{2} = z'$, the above equation will change to

$$Q = \int\int q_{i-1}\left(z' - u\right) q^{\dagger}_{N+1-i}\left(z'\right) g\left(z' - \frac{u}{2}, u\right) dz' du \tag{3.62}$$

where the integral is performed over the position of the end of the rods instead of the centres in contrast to equation 3.62. With a closer look, we can make further changes on the above equation

$$Q = \int q^{\dagger}_{N+1-i}(z') \left[\int q_{i-1}(z' - u) g\left(z' - \frac{u}{2}, u\right) du\right] dz' \tag{3.63}$$

The equation in the bracket is the convolution integral showed in equation 3.52. By substitution we obtain,

$$Q = \int q^{\dagger}_{N+1-i}(z') q_{i-1}(z') dz' \tag{3.64}$$

Equation 3.61, 3.62 and 3.63 are three different ways to calculate the partition function and they must result in the same value. This has been done as a method to test and validate the computer code.

From the probability density (equation 3.60), the total concentration at each position can be calculated

$$\rho_p(z) = \sigma \sum_{i=1}^{N} \int P_i(z,u) du \tag{3.65}$$

or,

$$\rho_p(z) = \sigma \sum_{i=1}^{N} \int \frac{q_{i-1}\left(z - \frac{u}{2}\right) q^{\dagger}_{N+1-i}\left(z + \frac{u}{2}\right) g(z,u)}{Q} du \tag{3.66}$$

where σ is called the grafting density and it equals the number of grafted chains per unit area of the surface. Note that conservation of material implies

$$\int \rho_p(z) dz = \sigma N \tag{3.67}$$

In brief, the steps that are taken to do the calculations are as follows. First, the average fields due to the interactions are specified either from an initial guess or previous calculations. Note that, so far, we have only shown the calculation related to the molecular field. The liquid crystalline field has not been introduced into the system yet. Once the field is known, the propagators are calculated and are used to find the partition function and concentration profile from the equations that are introduced in this section. The data from the previous step are used to check the self-consistent condition, which are set for our specific system. If the condition is not satisfied, the field must be corrected. A proper error tolerance is defined for the variance between the two fields. The process will iterate until the desired precision criteria is met. These equations, which are solved in this manner are said to be solved self-consistently and are done using numerical methods suited to the problem.

In the following sections, we will first discuss two different methods to incorporate a solvent into the system: implicit and explicit solvent. Next, a model for conventional polymer brush system (without liquid crystallinity) will be derived and validated by comparing to an analytical calculation from a theory called strong-stretching theory. Afterwards, the liquid crystalline field is introduced into the calculations and the formulas will be derived for this new case.

3.8 Solvent models

In order to incorporate the solvent interactions into the system, the implicit and explicit solvent methods can be used. The implicit solvent method assumes that the solvent is a continuous medium and the concentration of the polymer is low enough to assume that the system is in dilute regime. By using the incompressibility condition ($\rho_s(z) = 1 - \rho_p(z)$), the degrees of freedom of solvent molecules are integrated out. The effect of solvent molecules is incorporated implicitly in the calculations by introducing an effective pairwise interaction

between the solute molecules (polymer segments in our case) [23]. Although this approach is only accurate for dilute systems, it can provide a general insight about the behaviour of the system, while it is computationally cheap.

The explicit solvent method is a more accurate approach since it directly calculates the interactions between the solute molecules (polymer segments) and solvent. This method can be used for both dilute and concentrated systems. In the context of the field theoretic model, this is done by introducing a mean-field that acts on the solvent molecules [22]. By explicitly including the solvent interactions, we will derive a more realistic model. However, it is computationally more expensive. We will begin with the implicit solvent method and then extend the calculations to explicit solvent approach.

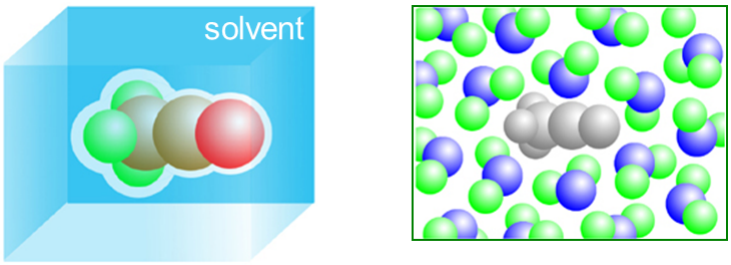

Figure 3.8: Implicit and explicit solvent. The figure on the left shows the implicit solvent case, where solvent is treated as a continuous medium. The figure on the right shows the explicit solvent case, where the molecular details of the solvent molecules are calculated explicitly. Reprinted from [24]

3.9 Model for conventional brushes with implicit solvent

To implicitly consider the solvent influence, a pair potential of mean force is defined for the polymer segments based on the Flory-Huggins theory (section 3.3). However, instead of using the lattice model described in the original Flory-Huggins theory, our model represents the Flory-Huggins interaction model in the context of the off-lattice field theory. The pairwise interaction is defined as

$$\frac{U}{k_B T} = \chi_{pp} \int \rho_p(z') f(z - z') \rho_p(z) dz dz' \tag{3.68}$$

where $f(z-z')$ defines the range of the interaction. By defining

$$w(z) = \chi_{pp} \int \rho_p(z') f(z-z') dz' \tag{3.69}$$

the pairwise interaction can be expressed as

$$\frac{U}{k_B T} = \int w(z) \rho_p(z) dz \tag{3.70}$$

where χ_{pp} is the polymer-polymer interaction parameter, $\rho_p(z)$ is the concentration of polymer and $w(z)$ is the dimensionless mean field that represents the isotropic interactions between polymers. As shown before, the concentration of the rigid rod is calculated based on the position of the center of the rods. The finite size of the rods implies that the range of interactions should be comparable to a. For the simple range of the interactions, we assume the Gaussian distribution

$$f(z-z') = \frac{\exp\left(\frac{-(z-z')^2}{2\sigma'^2}\right)}{\int \exp\left(\frac{-(z-z')^2}{2\sigma'^2}\right) dz} \tag{3.71}$$

σ'^2 is the variance and it is set to 0.9 for long chains.

Equation 3.69 is a self-consistent condition that needs to be satisfied in our calculation. For convenience, we define the smeared concentration

$$\rho_{sm}(z) = \int \rho_p(z') f(z-z') dz' \tag{3.72}$$

such that the SCFT condition is simply

$$w(z) = \chi_{pp} \rho_{sm}(z) \tag{3.73}$$

As mentioned before, calculations starts with an initial condition for the fields. From that, the propagators, partition function and average concentration are calculated. Next, the concentration profile is checked to see if it satisfies equation 3.73. If not, the average field is corrected and the previous steps are repeated. This is done repetitively until the self-consistency condition is satisfied up to a precision criterion that is set beforehand.

Results from this section are for conventional brushes where no liquid crystalline field acts on the molecules. Conventional brushes have already been studied thoroughly. A theory called strong-stretching theory (SST) leads to an analytical solution for non-LCP brushes that can be compared to our numerical calculation. This comparison can validate our calculations. This theory along with its analytical calculations are explained in the following section and the result of the comparison with our data can be found in Chapter 5.

3.9.1 Strong-stretching theory (SST): Analytical approximation for conventional polymer brushes

Strong-stretching theory provides an analytical approximation by assuming that the chains are extremely stretched that no tension exists at the free end of the chains $z = z_0$. Based on this assumption, an analogy with classical mechanics is made which equates a polymer chain with a particle that starts at rest and arrives at the grafting surface exactly after one unit of time regardless of its starting position z_0 (analogous to a pendulum). With this analogy, a mean field is derived [25]

$$w_{sst}(z) = \frac{3\pi^2(L^2 - z^2)}{8a^2N} \tag{3.74}$$

where N is the degree of polymerization (in our case, the number of rods) and a is the segment length (rod length). In SST, the brush has a well-defined absolute thickness given by

$$L = (\frac{4\nu\sigma}{\pi^2 a\rho_0})^{\frac{1}{3}} aN \tag{3.75}$$

where $\nu = 1 - 2\chi$ (χ is the Flory-Huggins interaction parameter), σ is the grafting density, ρ_0 is the segment concentration of a pure melt. From the field, the concentration and end segment distribution is found to be [25]

$$\rho(z) = \frac{3(L^2 - z^2)aN^{\frac{1}{2}}}{2L^3}, \tag{3.76a}$$

$$\rho_{end}(z_0) = \frac{3z_0 aN^{\frac{1}{2}}}{L^3}\sqrt{L^2 - z_0^2} \tag{3.76b}$$

Based on these calculations, strong stretching theory predicts that the concentration profile of a polymer brush with sufficient thickness has a parabolic shape in general (see Figure 3.9) [25]. For moderate thickness, the concentration profile deviates from the SST prediction in two regions. One is the tail region towards the end of the brush and the other is the depletion layer next to the grafting surface. Additionally, this theory predicts that the free end of the chains has the distribution shown in Figure 3.10 throughout the brush. SST results will be compared to our numerical calculation in Chapter 5.

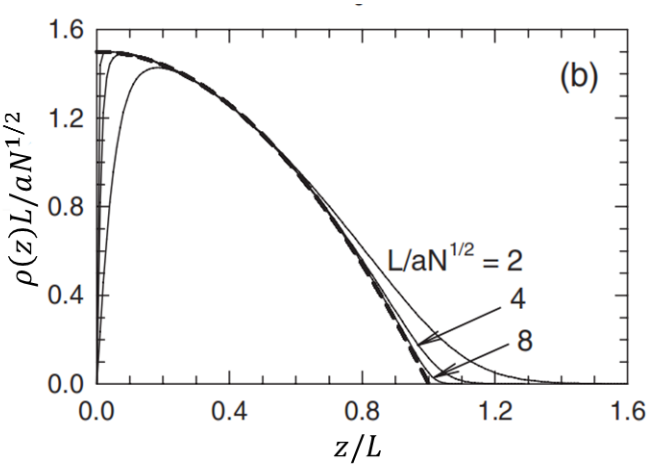

Figure 3.9: Dashed curve is the SST result (equation 3.76a) and solid curves are SCFT results using the continuous Gaussian chain model. For high thickness of the brush, the concentration of the polymers converge to the analytical approximations. Reprinted from [25]

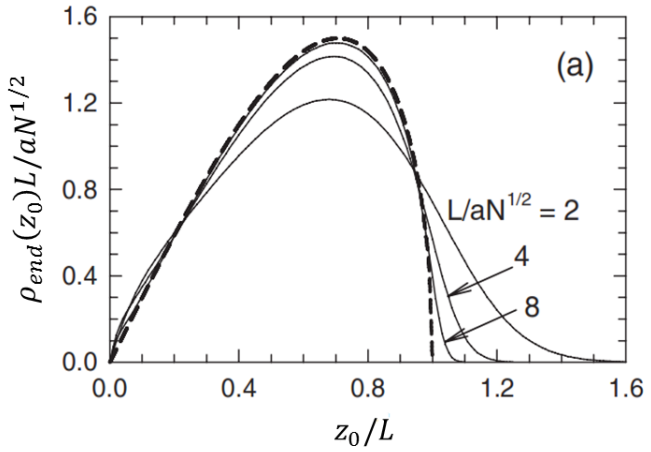

Figure 3.10: End segment distribution of polymer chains. Dashed curve is the SST result (equation 3.76b) and solid curves are SCFT results using the continuous Gaussian chain model. For high thickness of the brush, SCFT result converges to the SST solution. Reprinted from [25].

3.10 Model for LCP brushes with implicit solvent

Once the preliminary calculations for the conventional brush are done and validated, we move forward to add the liquid crystalline interactions in our system. Again, we make use of the mean-field approximation and introduce an ensemble-average field W_{LC} for the LC interactions. With that, equation 3.30 becomes

$$E = \sum_{i=1}^{N} b(\mathbf{u}_i) + \sum_{i=1}^{N} W(\mathbf{r}_i) + \sum_{i=1}^{N} W_{LC}(\mathbf{r}_i) P_2(\cos\theta_i) \tag{3.77}$$

where P_2 is the second Legendre polynomial. Following the same procedure as before, we find

$$g(z,u) = \frac{1}{2}\exp(-w(z) - w_{LC}(z)P_2(u)) \tag{3.78}$$

Based on the Maier-Saupe model, described in the previous chapter, the average liquid crystalline field must satisfy the following condition

$$w_{LC}(z) = -\epsilon \int f(z-z')S_2(z')\rho_p(z')dz' \tag{3.79}$$

where ϵ is the anisotropic coupling parameter (similar to χ for molecular interactions), $\rho_p(z)$ is the concentration of polymer segments, $S_2(z)$ is the order parameter and $f(z)$ is the function given in equation 3.71.

As explained in the Chapter 2, the order parameter quantifies how much order exists in the system, i.e.,

$$S_2 = \left\langle \frac{3\cos^2\theta - 1}{2} \right\rangle = \langle P_2(\cos\theta)\rangle \tag{3.80}$$

The procedure to find the LC field, $w_{LC}(z)$, is similar to obtaining the isotropic molecular field, $w(z)$. An initial guess is used for $w_{LC}(z)$ and $w(z)$, and then the probability density and concentration are calculated. Next the order parameter is determined. Note that in our case the order parameter is a function of distance from the grafting surface

$$S_2(z) = \frac{\frac{1}{N}\sum_{i=1}^{N}\int_{-1}^{1} P_2(u)P_i(u,z)du}{\frac{1}{N}\sum_{i=1}^{N}\int_{-1}^{1} P_i(u,z)du} \tag{3.81}$$

where N is the total number of the rods, $P_2(u)$ is the second Legendre polynomial and P_i is the probability density for the i^{th} rod as before. Note that the term in the denominator is used to normalize the calculation. If we multiply the nominator and denominator by σN

$$S_2(z) = \frac{\sigma \sum_{i=1}^{N} \int_{-1}^{1} P_2(u) P_i(u,z) du}{\sigma \sum_{i=1}^{N} \int_{-1}^{1} P_i(u,z) du} \tag{3.82}$$

The expression in the denominator is the same as equation 3.65. Thus, it is equal to the position-dependent concentration. So,

$$\rho(z) S_2(z) = \sigma \sum_{i=1}^{N} \int_{-1}^{1} P_2(u) P_i(u,z) du \tag{3.83}$$

Once the concentration and the order parameter are found, they are used to check the conditions in equations 3.73 and 3.79. This is done iteratively until the conditions are satisfied.

3.11 Model for LCP brushes with explicit solvent

So far, we have studied our system with an implicit solvent. These results are important to gain insight about the proposed system. In this section, we explicitly take into account the solvent effect. This means that we define a new field to show the average molecular interactions between solvent molecules and polymer segments. In this approach, similar to the previous method, the parameter χ is employed to indicate the local interactions between polymer and solvent molecules. Additionally, the solution is assumed to be incompressible. Thus, this method follows the interaction model and incompressibility assumption of the Flory-Huggins theory [23]. The energy due to the average interactions of a solvent molecule at z is

$$E_s = W_s(z) \tag{3.84}$$

Based on the Flory-Huggins model and above explanation, this field is found to be

$$w_s(z) = \chi \int f(z - z') \rho_p(z') dz' + \xi(z) \tag{3.85}$$

$w_s(z)$ is the dimensionless form of the $W_s(z)$ introduced in equation 3.58. The interaction field for polymer segments would change to

$$w_p(z) = \chi \int f(z - z')\rho_s(z')dz' + \xi(z) \tag{3.86}$$

where $f(z)$ is defined in equation 3.71, ρ_p and ρ_s are the polymer and solvent concentrations, respectively. ξ is a field that enforces the incompressibility condition (upon normalizing the concentrations)

$$\rho_p(z) + \rho_s(z) = 1 \tag{3.87}$$

This is another self-consistent condition that needs to be satisfied by adjusting the fields. The polymer concentration is calculated as shown in the previous section. Since we had

$$\int \rho_p(z)dz = \sigma N \tag{3.88}$$

Conservation of materials requires

$$\int \rho_s(z)dz = L_b - \sigma N \tag{3.89}$$

where L_b is the size of our system in z direction. The solvent concentration can be found using the solvent field

$$\rho_s(z) = \frac{L_b - \sigma N}{Q_s} \exp(-w_s(z)) \tag{3.90}$$

where

$$Q_s = \int \exp(-w_s(z))dz \tag{3.91}$$

is the partition function for a single solvent molecule in the field.

Here again we start with an initial guess for $w_s(z)$, $w_p(z)$ and $w_{LC}(z)$. Using that, concentrations are calculated. Next, we need to check the incompressibility condition (equation 3.87) and self-consistent condition for liquid crystalline field (equation 3.79). Calculations are repeated until the fields are adjusted so that the conditions are satisfied. Note that here we have a non-LC solvent since the LC field does not act on the solvent molecules. With this model, we looked at one special case of good solvent, where $\chi = 0$. This case, which is called an athermal solvent, assumes that solvent molecules and polymer segments have similar interactions. When $\chi = 0$, the only term that needs to be satisfied in equation 3.85 and equation 3.86 is the pressure field that enforces the incompressibility condition.

So far, we have demonstrated the method to calculate different parameters in our system and find different configurations of the polymer chains. In order to determine the stability of each configuration and compare different solutions, it is required to calculate the free energy associated with each of these configurations. This will lead us to plot a phase diagram based on the system parameters. The next section will show the free energy calculations in detail.

3.11.1 Free energy calculation

In equilibrium, the system settles to the phase (or state) with the minimum free energy. To find this stable phase, we calculate the free energy associated with each configuration and determine the minimum. The free energy of n_p polymers and n_s solvent molecules is

$$\begin{aligned}\frac{F}{Vk_BT} &= -\frac{\sigma}{L_b}\ln\mathcal{Q}_p - \left(1-\frac{\sigma N}{L_b}\right)\ln\mathcal{Q}_s \\ &- \frac{1}{L_b}\int[w_p(z)\rho_p(z) + w_s(z)\rho_s(z) + w_{LC}\rho_p(z)S_2(z)]dz \\ &+ \frac{\chi}{L_b}\int f(z-z')\rho_p(z)\rho_s(z')dzdz' \\ &- \frac{\epsilon}{2L_b}\int f(z-z')\rho_p(z)S_2(z)\rho_p(z')S_2(z')dzdz' \end{aligned} \tag{3.92}$$

where $V = Nn_p + n_s$ is the total dimensionless volume of the system.

Based on statistical mechanics, the logarithms of the partition functions in equation 3.92 yield the total free energy of a single chain in the field. The first integral removes the average energy of each field. The second integral follows the Flory-Huggins model and adds the pairwise energy of solvent and polymer segments. The last integral follows the Maier-Saupe model and counts the pairwise anisotropic interactions between the polymer segments.

Note that by adding a constant to the molecular field such that $w(z) \to w(z) + c$, the function $g(z,u)$ and propagators change to

$$\begin{aligned} g_{\text{new}}(z,u) &= \frac{1}{2}\exp\left(-w_{LC}P_2(u) - (w+c)\right) \\ &= g_{\text{old}}(z,u)\exp\left(-c\right) \\ q_{\text{new},i}(z) &= \exp\left(-ic\right)q_{\text{old},i}(z) \\ q^\dagger_{\text{new},i}(z) &= \exp\left(-(N-i+1)c\right)q^\dagger_{\text{old},i}(z) \end{aligned} \tag{3.93}$$

Thus, the new partition function becomes

$$Q_{\text{new},p} = \exp(-Nc)\, Q_{\text{old},p} \tag{3.94}$$

When these new quantities are substituted in equation 3.92, the constant factors of $\exp(-c)$ cancel and the free energy remains unaffected (using equation 3.88). It is possible to obtain the same solution and configurations for different molecular fields due to this invariance [25]. Figure 3.11 indicates this situation.

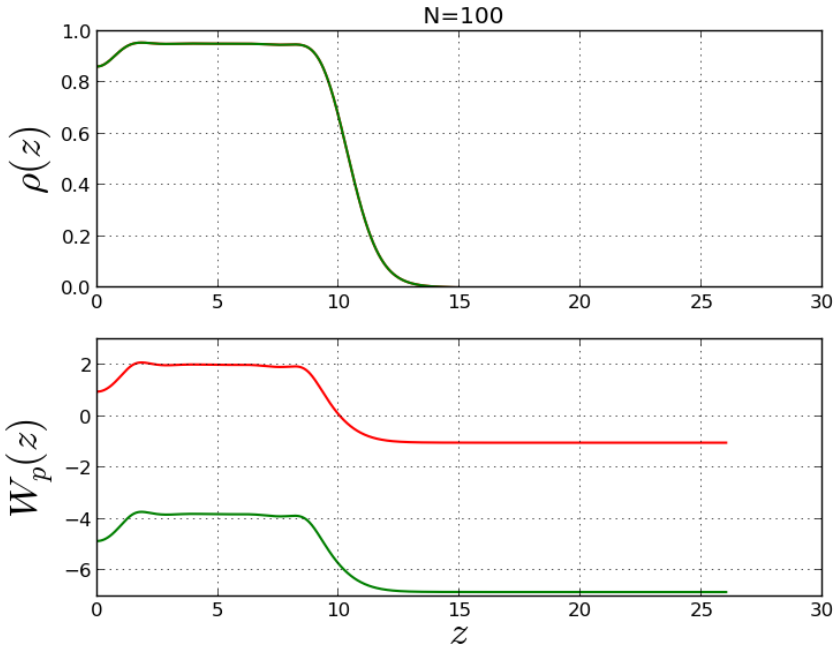

Figure 3.11: Concentration profile, $\rho_p(z)$, and molecular field, $W_p(z)$, for two systems. While the molecular fields in these systems are different from each other by a constant factor, the concentration profile for both systems are exactly the same.

In order to avoid this, it is required to put a constraint on the field. This can be done in several ways, but we chose to force the field to become zero at the end of the system box

$$w(L_b) = 0 \tag{3.95}$$

As evident in equation 3.92, the free energy depends on the grafting density, σ, anisotropic coupling parameter, ϵ, Flory-Huggins parameter, χ and the number of the rods, N. Thus,

we can calculate the free energy for different values of σ, ϵ and N (χ is set to zero since the solvent is assumed to be athermal). This can be represented by a phase diagram for our system, which is shown in Chapter 5. In the next chapter, we will discuss the numerical methods that are employed to solve the equations derived in this chapter.

Chapter 4

Numerical calculation

4.1 Numerical methods

In order to transform our models and equations into a discrete scheme, the length of the box L is divided into L units. Each unit is then discretized into A grid points. Thus, a total of LA uniform grid points is defined and the calculations are done based on them.

It is shown in the previous section that our calculations start off with evaluating the propagators with a convolution integral. Additionally, partition functions, smeared concentrations and the free energy are determined by calculation of integrals. Several methods of numerical integration exist that have different accuracy and applicability. Here we apply the most well-known and commonly used technique called the composite trapezoidal rule. The trapezoidal method has a very simple formula. This technique approximates the integral of function $f(x)$ as a discrete sum of areas of trapezoids. If we have a uniform partition in interval $[a, b]$, where

$$\begin{aligned} &a = x_0 < x_1 < ... < x_n = b \qquad \Delta x = \frac{b-a}{n} \\ &x_i = a + i\Delta x \quad 0 \leq i \leq n \end{aligned} \tag{4.1}$$

then the trapezoidal formula would be [26]

$$\int_a^b f(x)dx = \frac{b-a}{2n}\left[f(a) + 2\left[\sum_{i=1}^{n-1} f(a+i\Delta x)\right] + f(b)\right] \tag{4.2}$$

Although the trapezoidal rule is second-order accurate, it becomes precise for a sufficiently high number of grid points.

Another numerical scheme that has been employed in our calculations is the Newton-Raphson method. This method is an iterative technique to locate the root of a real-valued function. If the function $f(x)$ has a non-zero first derivative, $f'(x)$, then the initial guess x_0 for the root of the function $f(x)$ can be improved as follows [26]

$$x_1 = x_0 - \frac{f(x_0)}{f'(x_0)} \tag{4.3}$$

In fact, x_1 is the intersection between the x axis and tangent of the graph $f(x)$ at the point $(x_0, f(x_0))$. The iteration

$$x_{n+1} = x_n - \frac{f(x_n)}{f'(x_n)} \tag{4.4}$$

is repeated until the desired accuracy is reached

$$|x_{n+1} - x_n| < \text{tolerence} \tag{4.5}$$

This method is useful to find the transition point in the free energy diagram. Let us name the free energies associated with two different configurations to be $F_1(\epsilon)$ and $F_2(\epsilon)$ in which ϵ is the anisotropic coupling parameter. We are looking for the ϵ where F_1 and F_2 intersect. Thus, $f(\epsilon)$ is defined as

$$f(\epsilon) = F_1(\epsilon) - F_2(\epsilon) \tag{4.6}$$

and the Newton-Raphson scheme would be

$$\epsilon_{n+1} = \epsilon_n - \frac{f(\epsilon_n)}{f'(\epsilon_n)} \tag{4.7}$$

The derivative needs to be approximated

$$f'(\epsilon_n) \approx \frac{f(\epsilon_n + \Delta) - f(\epsilon_n - \Delta)}{2\Delta} \tag{4.8}$$

The Newton-Raphson method significantly improves the speed of calculations in finding the transition points and creating the phase diagram.

4.2 Solving a non-linear system of equations

4.2.1 Simple-mixing method

As highlighted previously, the calculations start with an initial guess for the fields. Following that, the propagators and the concentrations are determined. Finally, self-consistent

conditions are checked to determine how close the initial guesses are to the solution. The simple-mixing method is an iterative procedure that continues to correct the field until we reach to the solution where all the desired conditions are satisfied [27]. As mentioned before, two self-consistent conditions must be satisfied in order to find the correct solutions, i.e.,

$$\begin{aligned} &\rho_p(z) + \rho_s(z) = 1 \quad \text{Incompressibility condition} \\ &w_{LC}(z) = -\varepsilon \int f(z - z')S_2(z')\rho_p(z')dz' \end{aligned} \tag{4.9}$$

In the simple-mixing method, the initial molecular field is corrected by adding the difference from unity of the total concentration multiplied by a relaxation parameter to the previous field

$$w^{k+1}(z) = w^k(z) + \lambda(\rho_p + \rho_s - 1) \tag{4.10}$$

where k is the iteration number and λ is the relaxation parameter. It is an arbitrary positive number, small enough to ensure stability (it is usually 0.1 or less). Based on equation 4.9, $\rho_p + \rho_s = 1$ and $w^{k+1}(z) = w^k(z)$ if the field is correct. Otherwise, it is corrected until the proper field is found. Note that in the case of an implicit solvent, where no solvent concentration appears in the model, equation 4.10 changes to

$$w^{k+1}(z) = w^k(z) + \lambda(\chi_{pp} \int \rho_p(z')f(z - z')dz' - w^k(z)) \tag{4.11}$$

Since the self-consistent field condition $w(z) = \chi_{pp} \int \rho_p(z')f(z - z')dz'$ must be satisfied.

The same approach is used for the liquid crystalline field. The simple-mixing scheme would be as follows

$$w_{LC}^{k+1}(z) = w_{LC}^k(z) + \lambda(-\epsilon \int f(z - z')S_2(z')\rho_p(z')dz' - w_{LC}^k(z)) \tag{4.12}$$

With this, we can come up with the general formula for the simple-mixing method. If the self-consistent condition is satisfied by $w_{out}(z)$ and the initial field is $w_{in}(z)$, then the general formula would be

$$w_{in}^{k+1}(z) = w_{in}^k(z) + \lambda(w_{out}^k(z) - w_{in}^k(z)) \tag{4.13}$$

This method of correction is repeated iteratively until the error becomes less than a tolerance that is previously set. In general, the error is calculated as

$$Error = \left[\frac{1}{L}\int_0^L (w_{out}(z) - w_{in}(z))^2 dz\right]^{\frac{1}{2}} \tag{4.14}$$

Although the simple-mixing method is easy to implement, it can take a large number of iterations before it converges to the correct solution. This is specially troublesome when a high level of accuracy (set by the tolerance) is required. Another method called Anderson-mixing exists that highly increases the speed of convergence. Details related to this method is explained in the next section.

4.2.2 Anderson-mixing method

As explained in the previous section, the simple-mixing method may take several iterations before converging to the proper fields. Anderson-mixing method improves the simple-mixing method by combining information from previous steps (histories). In order to illustrate the Anderson-mixing method, we continue to use notations from the previous section, where the self-consistent condition is called $w_{out}(z)$ and the initial field is $w_{in}(z)$. In Anderson-mixing, a deviation is defined as [28]

$$d^k(z) = w^k_{out}(z) - w^k_{in}(z) \tag{4.15}$$

where k is the iteration step. Next an error is defined as follows

$$Error = \left[\frac{\sum\limits_j (d^k(z_j))^2}{\sum\limits_j (w^k_{in}(z_j))^2} \right]^{\frac{1}{2}} \tag{4.16}$$

Note that the above error is calculated for both the molecular field and LC field. The sum of both errors must be less than a tolerance. Otherwise, we correct the fields. In Anderson-mixing, this is done by evaluating a symmetric matrix and a vector from the preceding n_r iterations

$$U_{mn} = \sum_j (d^k(z_j) - d^{k-m}(z_j))(d^k(z_j) - d^{k-n}(z_j)) \tag{4.17}$$

$$V_m = \sum_j (d^k(z_j) - d^{k-m}(z_j))d^k(z_j) \tag{4.18}$$

where $n, m = 1, 2, 3, ..., n_r$. Using these two quantities, coefficients are found

$$C_n = \sum_m (U^{-1})_{mn} V_m \tag{4.19}$$

Now we combine the previous histories

$$w_c^k(z) = w^k(z) + \sum_{n=1}^{n_r} C_n(w^{k-n}(z) - w^k(z)) \tag{4.20}$$

$$D_c^k(z) = d^k(z) + \sum_{n=1}^{n_r} C_n(d^{k-n}(z) - d^k(z)) \tag{4.21}$$

The corrected fields are obtained from

$$w^{k+1}(z) = w_c^k(z) + \lambda D_c^k(z) \tag{4.22}$$

One way to employ the Anderson-mixing method in SCFT calculations is to use the initial histories from the simple-mixing method [28] and then switch to the Anderson-mixing and set $\lambda = 1$. This approach is applied since convergence does not occur when the number of the histories is small. Additionally, simple-mixing iterations are usually slow and computationally expensive. Thus, another technique exists that applies the Anderson-mixing from the very beginning [29]. In this method, the mixing parameter gradually increases as the number of histories reaches to a maximum n_h. In order to do this, we set $\lambda = 1.0 - 0.9^k$ and $n_r = \min(k-1, n_h)$. In our calculations, we set $n_h = 20$.

Chapter 5

Results and discussion

In this project, a field-theoretic model is derived for isotropic and anisotropic interactions in a system of liquid crystalline polymer brushes. Our model is able to predict the configuration and orientational order of polymers with different grafting density, chain length and liquid crystallinity.

In section 5.1, we compare our numerical calculations for a conventional (non-liquid crystalline) polymer brush with the analytical approximation derived from strong-stretching theory. Agreement between these results validates our preliminary calculations. Following this validation, the liquid crystalline field is added to the system. Results are divided into two sections based on the method of solvent incorporation.

The implicit solvent method is easy to implement since solvent is represented as a continuum medium and the model does not include the solvent degrees of freedom with the assumption that system is dilute. The interactions between solvent molecules and polymers are represented by an average pairwise potential between polymer segments. Although this method is an artificial representation of solvent interactions, it provides general insight into the system. Results for this method are shown in section 5.2. In this section we have studied the effect of each system parameter (isotropic and anisotropic interaction parameters and grafting density) on the configuration of the polymer chains.

The explicit solvent method is more realistic and accurate since it explicitly includes the solvent and polymer interactions. The average molecular interaction experienced by solvent molecules is represented by a new field, $w_s(z)$, and the incompressibility effect is taken into account. Results for this case are given in section 5.3. In this section, we will show different configurations of polymer chains along with their degrees of orientational

order. A free energy diagram is presented, which will be used to identify the stable phases, allowing us to construct a phase diagram.

5.1 Validation of the preliminary model: Comparison between SCFT and SST results

To start off, we can validate our calculations by comparing the SCFT solution for a conventional polymer brush (in the absence of any liquid crystalline field) with the analytical solution derived from strong-stretching theory. As mentioned in section 3.9.1, the analytical and numerical calculation of the polymer concentration and end-segment distribution should agree for sufficiently large brush heights [25]. The brush height, L, is defined as

$$\frac{L}{aN^{\frac{1}{2}}} = (\frac{4\nu\sigma}{\pi^2 a\rho_0})^{\frac{1}{3}} N^{\frac{1}{2}} \tag{5.1}$$

where ν is the excluded volume, σ is the grafting density, ρ_0 is the segment concentration in a pure melt and a is the bond length. Figure 5.1 shows the concentration profiles for different brush heights calculated with the SCFT method. The dashed line is the SST solution for the concentration profile, which is calculated by equation 3.76a.

As predicted by equation 3.76a, the concentration profile obtained by SCFT develop a parabolic shape and eventually converge to the SST calculation for sufficiently thick brushes [25]. When the brush thickness is not large enough, SCFT profiles exhibit two distinct differences from the SST predictions: a depletion layer is observed near the wall $z = 0$ and a tail region forms near $z = L$. The depletion layer occurs since it is assumed that the wall is impenetrable and neutral to the polymer and solvent molecules. Thus, entropic forces near the wall are responsible for this depletion layer in SCFT results. SST theory does not take into account the entropic forces near the surfaces and thus deviates from SCFT calculations in this region. Deviation in the tail region is due to a breakdown in the SST assumption [23]. As mention in section 3.9.1, SST theory assumes that the chains are extremely extended that no tension exists at the free end of the chains [25]. Thus, the brush thickness has a well-defined size. However, SCFT calculations are not based on this assumption and the density profile decreases smoothly in this case.

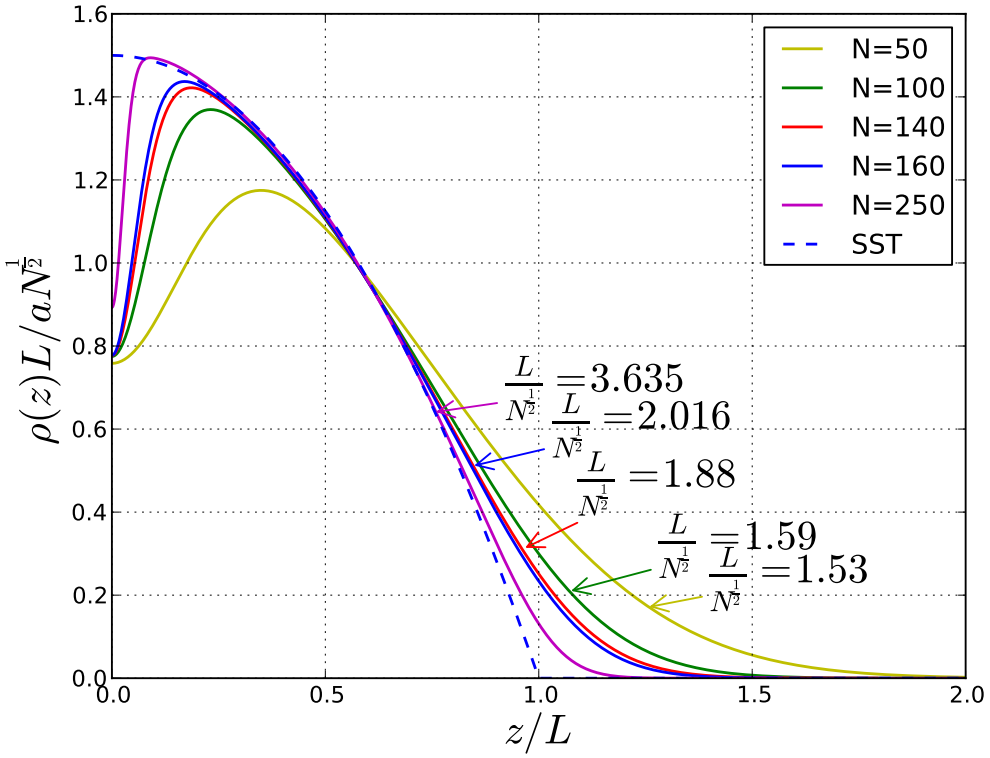

Figure 5.1: Comparison of concentration profiles determined by the SCFT and SST models. Solid curves are calculated with SCFT for various ratios of $L/N^{\frac{1}{2}}$, where L is the brush height and N is the number of the rods. The dashed curve shows the $L/N^{\frac{1}{2}} \to \infty$ limit predicted by SST. As can be seen, SCFT results converge to the SST calculation for sufficiently thick brushes.

Additionally, equation 3.76b predicts the distribution shown in Figure 5.2 for the end-segment concentration. Again, for sufficiently large brush heights, SCFT results converge to the SST prediction. For the same reasons mentioned above, deviation occurs at $z = 0$ and $z = L$ regions. Figures 5.1 and 5.2 show that our results approach the SST predictions for high brush thickness. This agreement validates the preliminary computer code for non-LCP brushes.

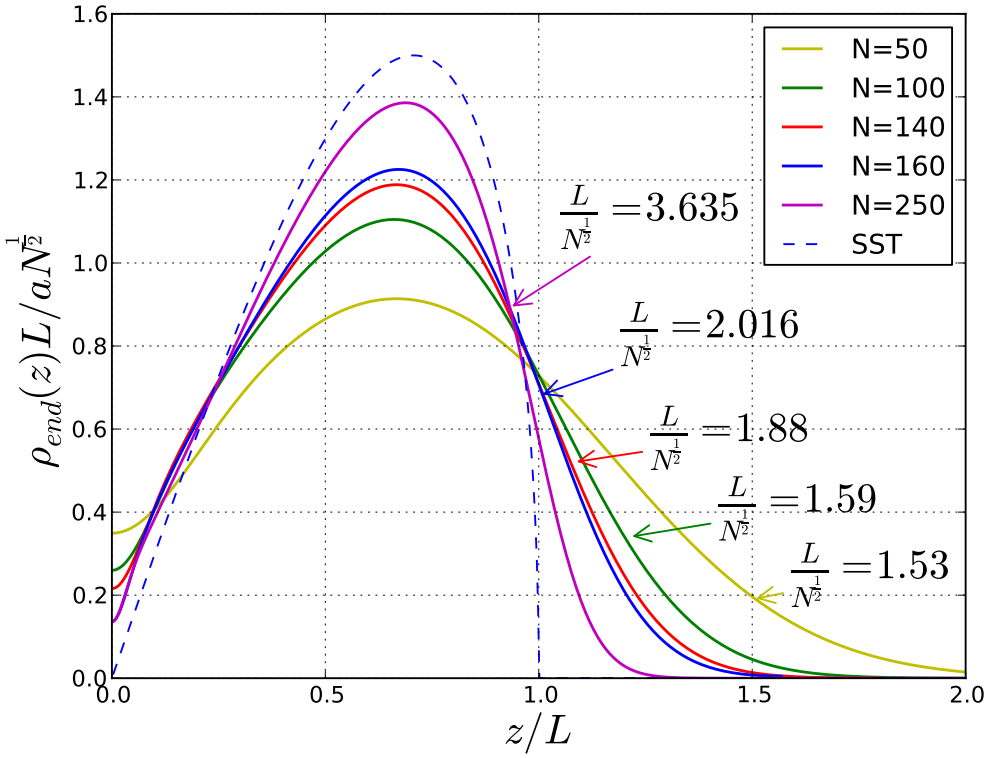

Figure 5.2: Comparison of the end-segment distribution of polymer chains determined by SCFT and SST models. Solid curves are calculated with SCFT for various ratios of $L/N^{\frac{1}{2}}$, where L is the brush height and N is the number of the rods. The dashed curve shows the $L/N^{\frac{1}{2}} \to \infty$ limit predicted by SST. As can be seen, SCFT results converge to the SST calculation for sufficiently thick brushes.

Next, the principles for LC brushes are introduced into the validated preliminary code. First, the results obtained using the implicit solvent model are examined. In this case, as explained in equations 3.73, 3.79 and 3.83, three parameters define the system: The Flory-Huggins parameter χ_{pp}, the grafting density σ and the anisotropic coupling parameter ϵ. In Figures 5.3-5.5, the effect of each parameter on the configuration of the system is studied.

5.2 Implicit solvent

This section presents results for the system of a LCP brush with an implicit solvent. As mentioned previously, the implicit solvent method assumes that the solvent is a continuous medium and the solvent-polymer interactions are taken into account by the interaction between polymer segments. In Chapter 3, we showed that for the implicit solvent case, two self-consistent conditions exist

$$w(z) = \chi_{pp} \int \rho_p(z') f(z - z') dz' \tag{5.2}$$

$$w_{LC}(z) = -\epsilon \int f(z - z') S_2(z') \rho_p(z') dz' \tag{5.3}$$

where the Flory-Huggins parameter, χ_{pp} controls the intermolecular interactions between polymer segments in the system, $\rho_p(z)$ is the polymer concentration, $f(z)$ is the smearing function defined in equation 3.71, ϵ is the anisotropic coupling parameter and $w_{LC}(z)$ is the liquid crystalline field due to anisotropic interactions between mesogens. Note that the polymer concentration depends on the grafting density, σ since

$$\int \rho_p(z) dz = \sigma N \tag{5.4}$$

In order to understand the general behaviour of the system, we will study the effect of each system parameter (χ_{pp}, ϵ and σ) on our system.

Effect of χ_{pp}

As previously mentioned, χ_{pp} is the polymer-polymer interaction parameter. Increasing χ_{pp} would result in a more stretched configuration. In fact, as the intermolecular interactions between polymer molecules become stronger, polymer chains tend to extend through the box to decrease the segment-segment interaction and avoid overlap. Figure 5.3 shows this behaviour. As can be seen in the concentration profile, $\chi_{pp} = 9$ is more stretched than the two other profiles with lower χ_{pp}.

The extended configuration would result in a higher degree of orientational order in the system. Thus, as indicated in the $S_2(z)$ profile in Figure 5.3, the degree of orientational order is higher for the extended configuration of $\chi_{pp} = 9$ compared to the other two cases with lower χ_{pp}. This figure also indicates that a high degree of orientational order exists

at very large z values. For instance, concentration profile for $\chi_{pp} = 1$ shows that there is a very low concentration (close to zero) at $z > 30$, while the $S_2(z)$ profile indicates a high order for chains at $z > 30$. In fact, any monomers that are positioned at $z > 30$ are from strongly stretched chains and thus have a high degree of order.

Note that, although polymer chains are stretched perpendicular to the wall, the degree of orientational order is generally low in this system (in Figure 5.3 the maximum of $S_2(z)$ is 0.14) compared to a highly ordered system where $S_2(z) = 1$. Additionally, the area under the concentration curve do not change since N and σ remain the same (equation 5.4).

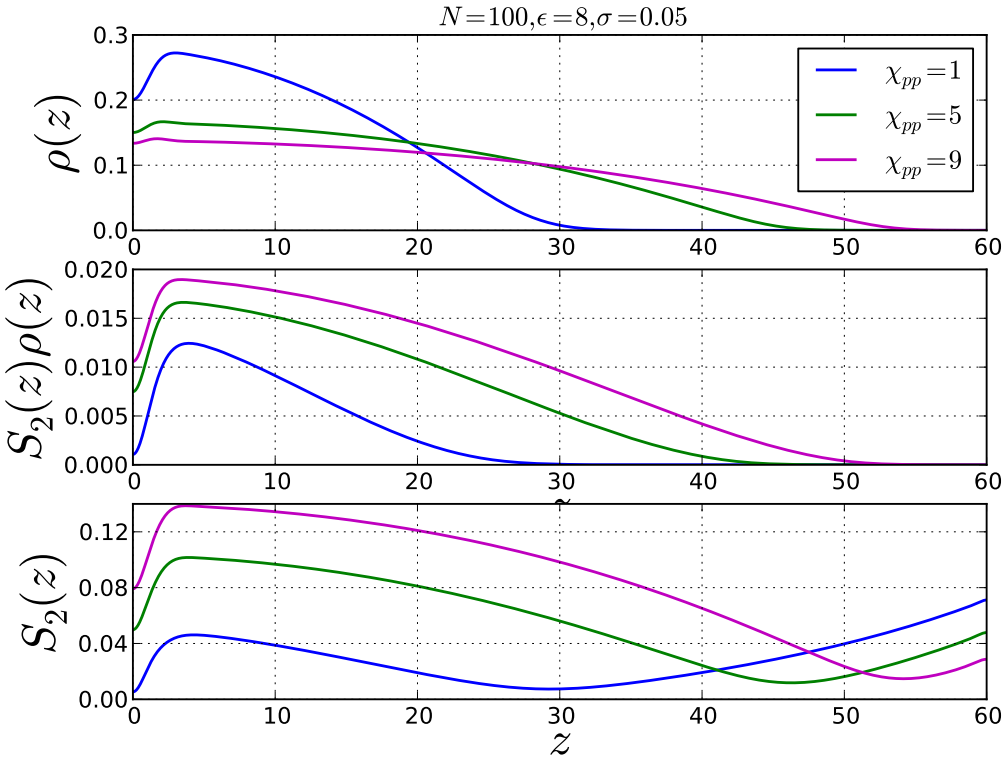

Figure 5.3: Effect of the polymer-polymer interaction parameter, χ_{pp}, on the configuration of polymer chains consisting of $N = 100$ freely-jointed rods with implicit solvent. ϵ and σ are the LC coupling parameter and grafting density, respectively. Concentration profiles, $\rho(z)$, indicate that polymer chains with higher χ_{pp} stretch away from the wall to avoid overlapping. The stretched configuration have a higher degree of orientational order as shown by profile for $S_2(z)$.

Effect of σ

The effect of grafting density, σ, on the chain configuration is also studied. Grafting density is the number of the grafted chains per unit area of the substrate. By increasing the grafting density, both isotropic and anisotropic interactions increase. Thus, polymer chains stretch away from the wall to avoid overlapping and increase the orientational ordering. Figure 5.4 shows this behaviour. Note that the area under the concentration curve increases as we increase the grafting density (equation 5.4).

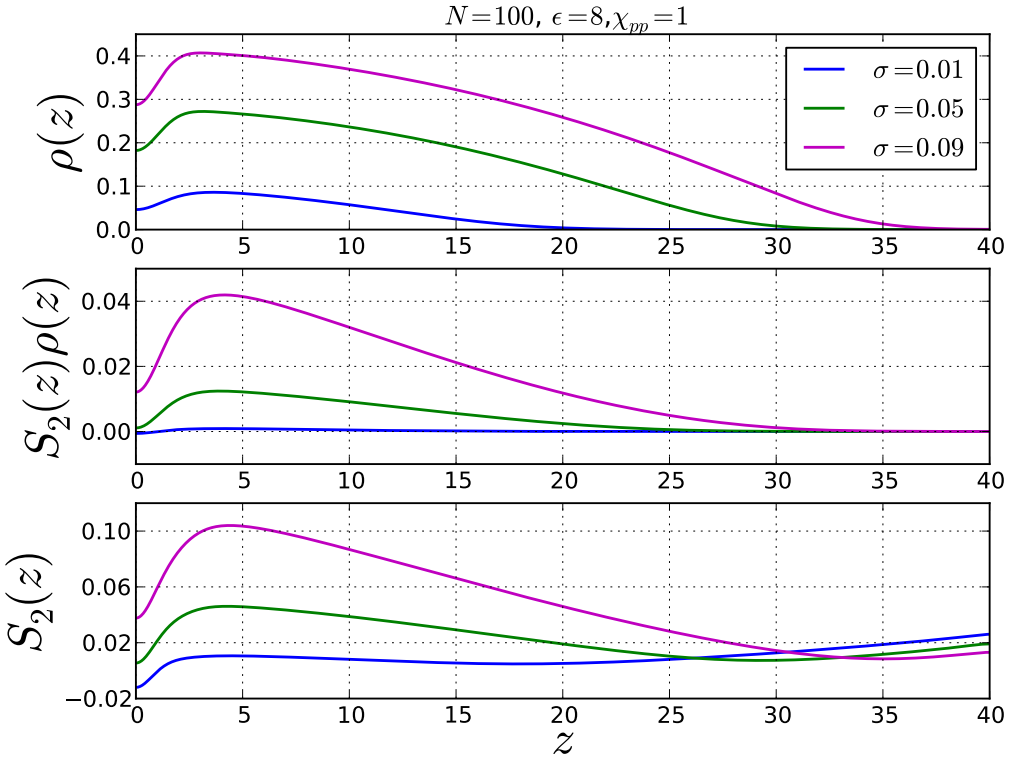

Figure 5.4: Effect of grafting density, σ, on the configuration of polymer chains consisting of $N = 100$ freely-jointed rods with implicit solvent. ϵ and χ_{pp} are the LC coupling parameter and Flory-Huggins interaction parameter, respectively. Increasing the grafting density increases the number of LC monomers, which results in an extended configuration. The extended configuration has higher degree of order as can be seen in the $S_2(z)$ profile.

Effect of ϵ

Another important system parameter is the anisotropic coupling parameter ϵ. As equation 5.3 shows, increasing ϵ would result in a stronger anisotropic field, which subsequently increases the orientational order in the system. As evident in Figure 5.5, increasing ϵ in the range of $(0-10)$ only changes the concentration profile very slightly. However, the order parameter diagram shows that for higher ϵ, the degree of orientational order increases in the system.

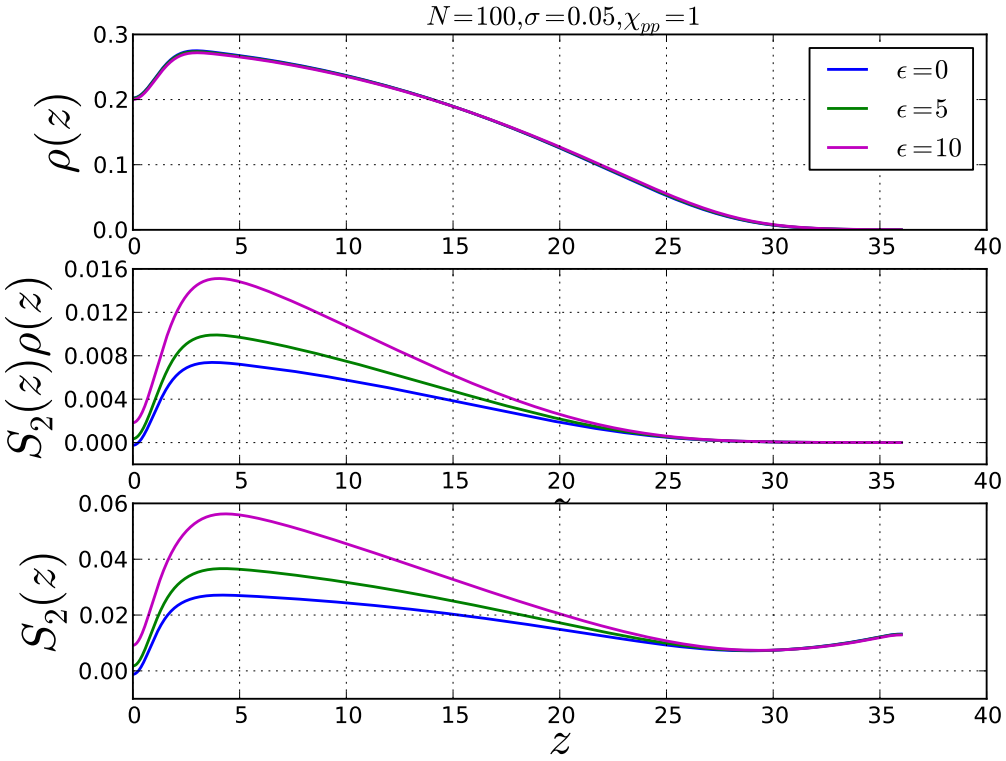

Figure 5.5: Effect of the LC coupling parameter, ϵ, on the configuration of polymer chains consisting of $N = 100$ freely-jointed rods with implicit solvent. σ and χ_{pp} are the grafting density and interaction parameter, respectively. Concentration profiles, $\rho(z)$, show that the effect of ϵ in the parameter regime of $(0-10)$ is not sufficiently strong to change the polymer configuration. However, as the $S_2(z)$ profile indicates, higher ϵ values force the chains to become more ordered.

In fact, the effect of ϵ over the range of $(0-10)$ is not strong enough to change the configuration of polymers. Thus, the phase shown in Figure 5.5 is stable in $(0-10)$ range. This phase is called the conventional brush (CB) phase since the concentration profile is no different from the $\epsilon = 0$ case. However, as demonstrated in the S_2 diagram, when the LC field is stronger (ϵ is higher), chains are forced to become ordered by choosing more backward steps (folding). Note that the degree of orientational order is generally low in this system (in Figure 5.5 the maximum of $S_2(z)$ is close to 0.06) compared to a highly ordered system, where $S_2(z) = 1$.

Another interesting point about Figure 5.5 is the case of $\epsilon = 0$. This case represents non-liquid crystalline polymer chains. Although no anisotropic interactions exist in non-LCP brushes, the degree of order is not zero as is shown in Figure 5.5. Molecules are slightly ordered since they possess an extended configuration due to the presence of the wall.

Note that the depletion layer that exists next to the wall in the concentration profiles of all the demonstrated diagrams is due to the entropic forces. In fact, depletion arises since chains tend to avoid the wall to be able to have more choices of configuration.

5.3 Explicit solvent

As explained before, the explicit solvent method is a more realistic approach for incorporating the solvent in the system. In this method, solvent is no longer a continuum and its interactions are calculated explicitly. In order to calculate the solvent interactions in the context of the field theoretic model, we introduced $w_s(z)$ as a field representing the intermolecular interaction of the solvent molecules (equation 3.85). Similar to the implicit case, $w_p(z)$ and $w_{LC}(z)$ are the fields for isotropic and anisotropic interactions experienced by polymer chains, respectively. Calculations for the explicit solvent method have been done for the athermal solvent case where $\chi = 0$. As mentioned before, the molecules of an athermal solvent are very similar to the monomers and has similar interactions. Using athermal solvent makes the explicit solvent calculations less computationally expensive since in this case, equations 3.85 and 3.86 reduce to

$$w_s(z) = w_p(z) = w(z) = \xi(z) \tag{5.5}$$

where $\xi(z)$ is the pressure field enforcing the incompressibility condition

$$\rho_p(z) + \rho_s(z) = 1 \tag{5.6}$$

Figure 5.6 shows the concentration profiles of solvent and polymer. As can be seen, the polymer is in the conventional brush (CB) phase, where it is extended over the box with a depletion layer next to the wall. The solvent concentration is also shown in this figure since the explicit solvent model is used (which takes into account the solvent degrees of freedom). It is clear that the total concentration in the system obeys the incompressibility condition (equation 5.6).

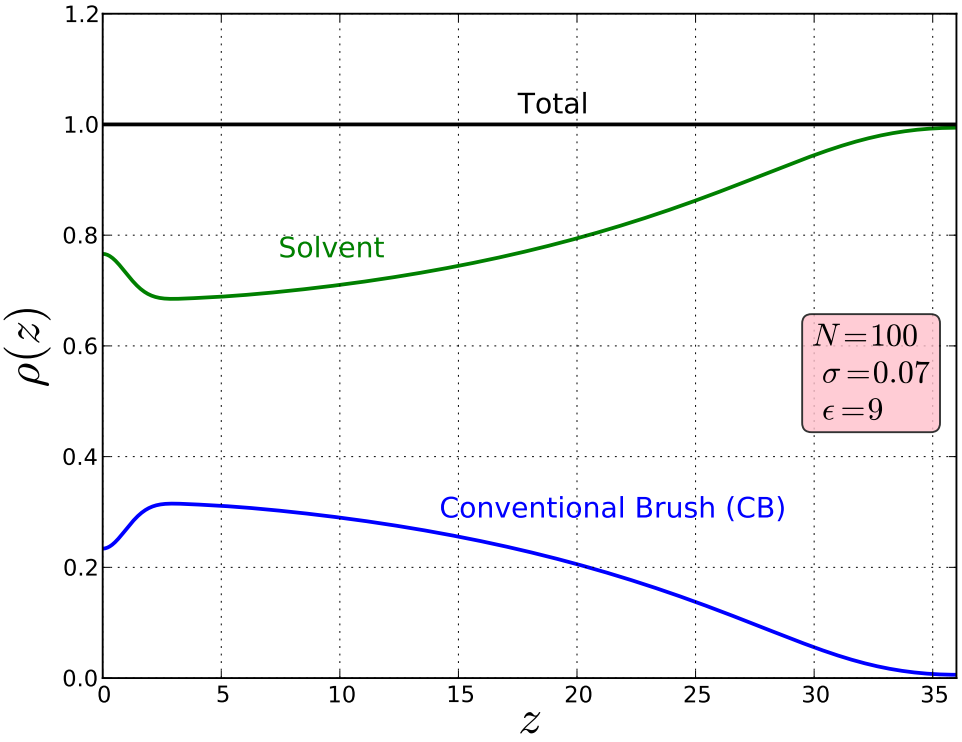

Figure 5.6: Concentration profiles for polymer, $\rho_p(z)$ and solvent, $\rho_s(z)$ in a system of polymer chains consisting of $N = 100$ freely-jointed rods with explicit solvent. σ and ϵ are the grafting density and the LC coupling parameter, respectively. In this configuration, which is called the conventional brush (CB), polymer chains extend through the box. The incompressibility condition forces the total concentration to be one.

As explained previously, in order to satisfy the self-consistent conditions and find the proper fields, we use an iterative method. The mean fields, $w(z)$ and $w_{lc}(z)$ are specified

with initial guesses, which are corrected iteratively until conditions 5.3 and 5.6 are satisfied. One should use variety of initial guesses in order to capture the solutions. By using a different structure as an initial guess for the fields (with the same set of parameters as before), a new solution was found. This new solution is shown in Figure 5.7. Note that all the system parameters (N, σ and ϵ) are the same as in the case shown in Figures 5.6 and 5.7. The only difference is the initial guess.

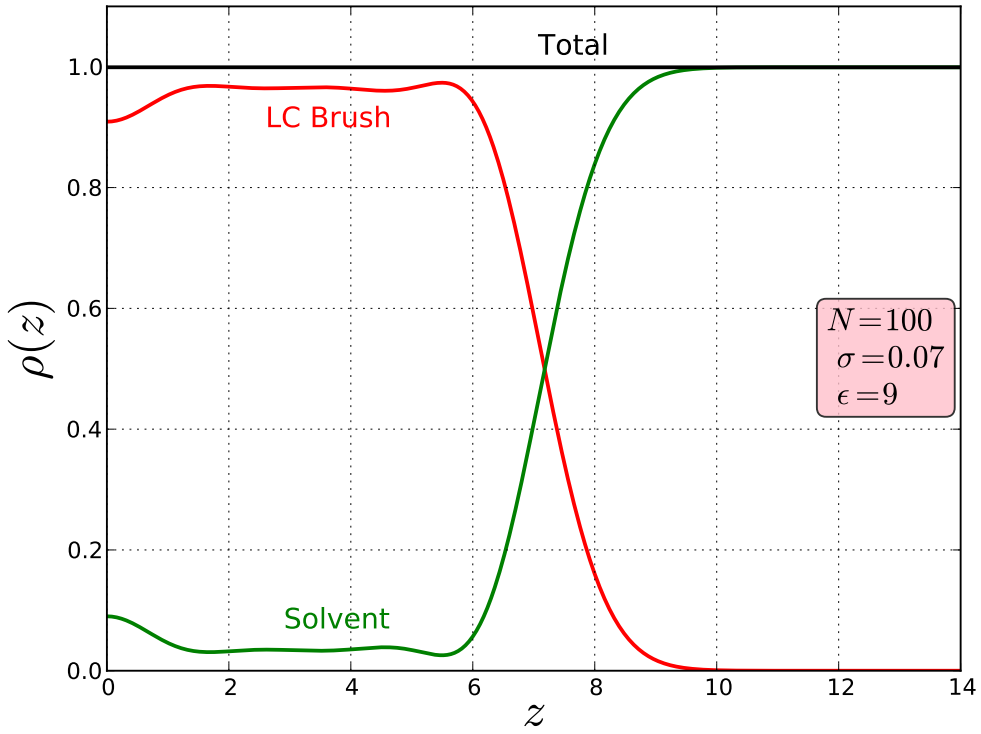

Figure 5.7: Concentration of the polymer, $\rho_p(z)$ and solvent, $\rho_s(z)$ in a system of polymer chains consisting of $N = 100$ freely-jointed rods with explicit solvent. σ and ϵ are the grafting density and the LC coupling parameter, respectively. In this phase, which is called liquid-crystalline (LC) brush, polymer chains collapse near the substrate and form a dense concentration profile. The incompressibility condition forces the total concentration to be one.

This new solution has a dense concentration near the grafting substrate. This con-

figuration is called a liquid-crystalline brush since it is highly ordered. The degree of orientational order is shown in Figure 5.8. As depicted, $S_2(z)$ is close to 1 near the wall. $S_2(z) \approx 1$ corresponds to the case where molecules are highly ordered and are parallel to the director, which is the z direction in our system. A highly-ordered dense concentration near the wall means that the polymer chains collapse in a zigzag manner. It is folding back and forth to maintain a high order by pointing towards the director (z direction).

Note that the LC phase is relevant in the context of the explicit solvent model. The implicit solvent model works best for dilute polymer solutions, where the concentration of polymers are low enough to model the solvent as a continues medium. In the LC phase, polymers are concentrated near the wall. Thus, the assumption that the system is dilute is violated. For this reason, we did not refer to the LC phase in previous section (implicit solvent).

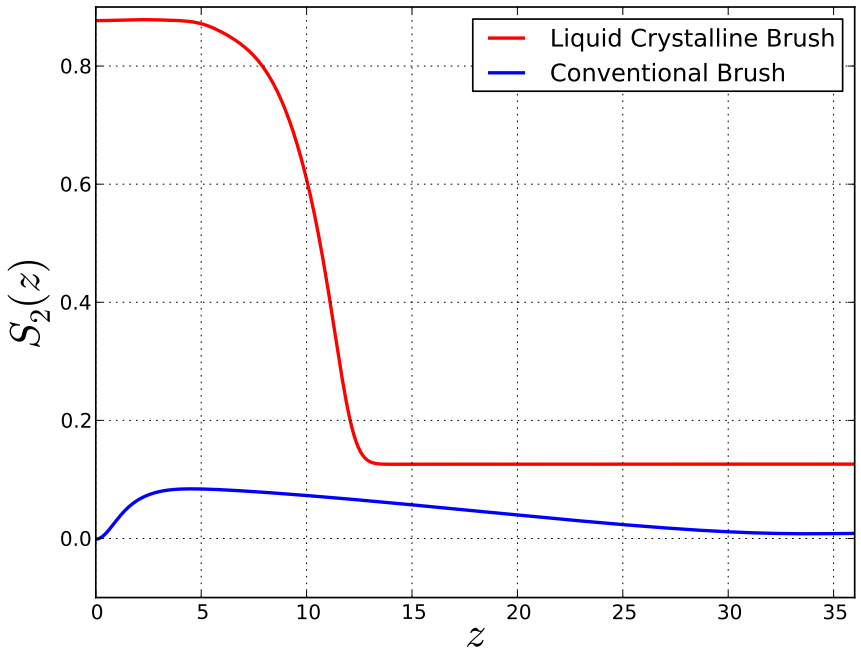

Figure 5.8: Degree of orientational order, $S_2(z)$, in the liquid-crystalline phase (LC) and the conventional brush (CB) phase. This diagram shows that the LC structure is highly ordered near the wall as $S_2(z)$ is close to one. In contrast, the conventional brush has an order close to zero throughout the box.

It is important to calculate the free energy associated with each configuration to understand the stable structure of polymer brushes for different system parameters. We start by considering the case of short chain polymers (15 rods) and then extend the calculations to long chains (100 rods).

Short chains

For short chains, we have found the two solutions that were discussed in the previous section, i.e., conventional and liquid crystalline brushes.

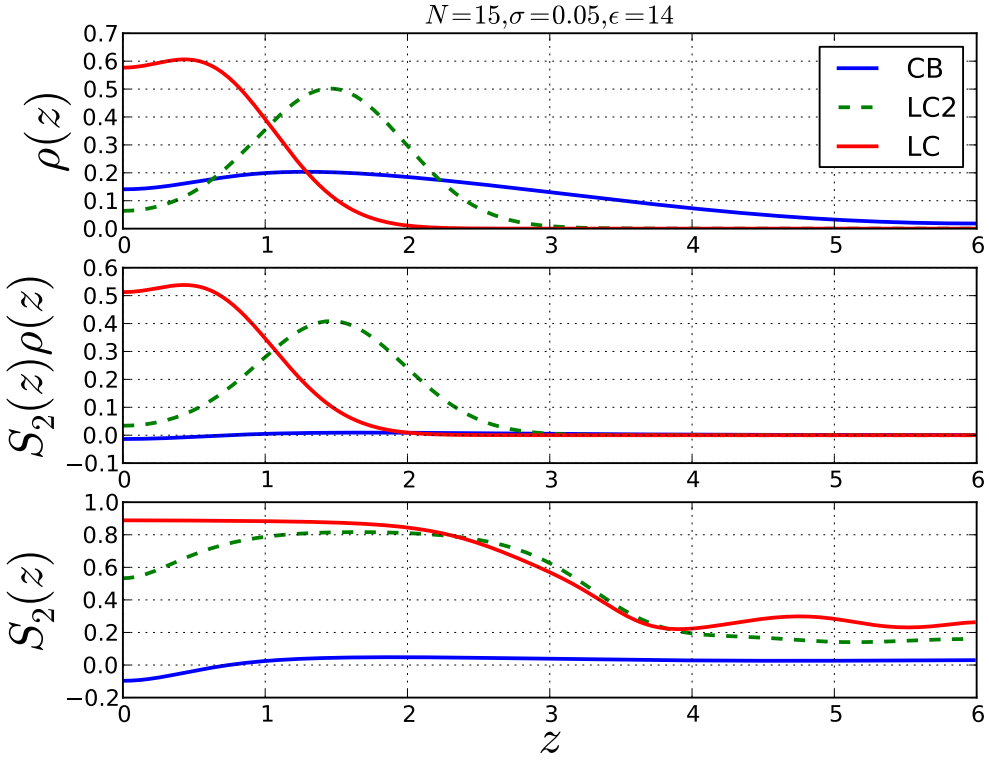

Figure 5.9: Three different configuration of polymer chains consisting of $N = 15$ rods. σ and ϵ are the grafting density and LC coupling parameter, respectively. The CB phase has an extended structure with a very low degree of order, $S_2(z) \approx 0$. In the LC phase, a dense brush is formed near the wall with $S_2(z) \approx 1$. The LC2 phase is similar to the LC phase but it is formed farther from the grafted surface.

While different initial guesses for the fields would lead to the LC or CB structure, it is possible to obtain a third solution that is also highly ordered. This third solution, which we called the second liquid crystalline (LC2) brush, is collapsed farther from the wall rather than immediately close to it (see Figure 5.9).

For each solution, we calculate the associated free energy using equation 3.92. This is done for a range of anisotropic coupling parameters, ϵ, in order to create a free energy diagram. Figure 5.10 shows the free energy diagram for the three solutions.

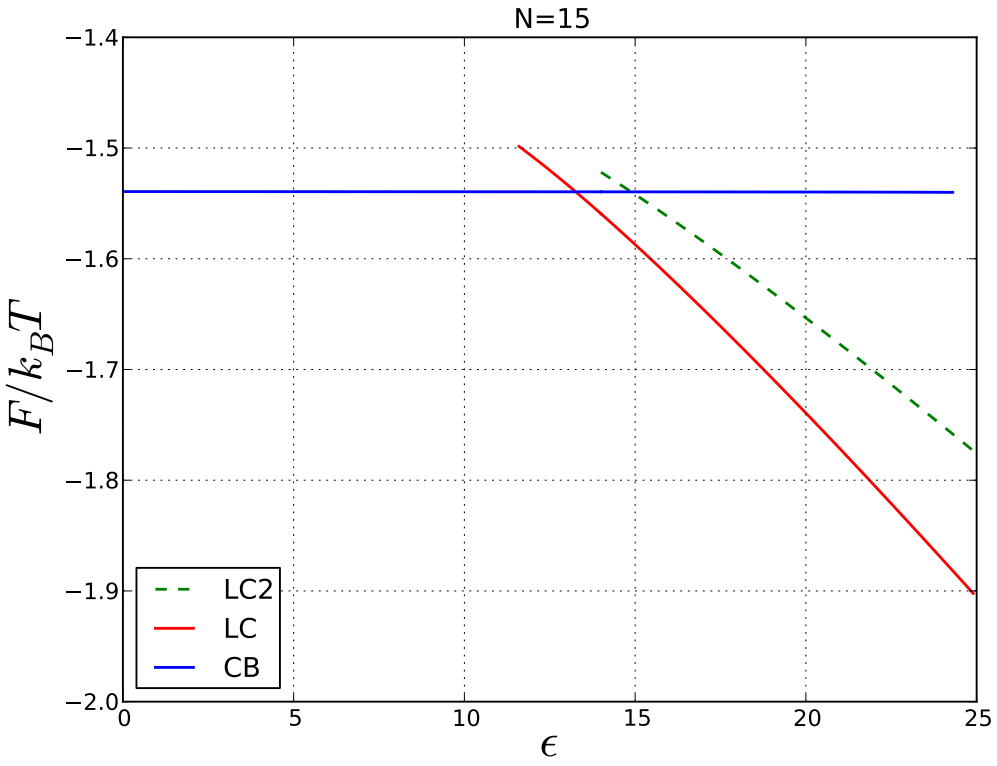

Figure 5.10: Free energy associated with three solutions found for short polymer chains $N = 15$, versus the anisotropic coupling parameter, ϵ. When the anisotropic interactions between polymer chains is strong (ϵ is high), the polymer chains form a highly ordered configuration and the LC phase becomes stable. For low ϵ, the isotropic interactions dominate and the CB solution is stable. LC2 solution is unstable for all the ϵ values.

It is evident in Figure 5.10 that for small ϵ where the LC field is weak, the CB config-

uration is most stable. The free energy over this interval is independent of ϵ. At higher ϵ, the LC solution becomes stable since the strong LC field forces the polymers to become ordered and collapse near the wall. The free energy decreases almost linearly as ϵ increases in this regime. The free energy associated with the LC2 structure is higher throughout the whole range of ϵ, which indicates that this phase is only metastable. In fact, we expect numerous unstable LC phases with ordered regions at different distances from the wall.

The calculations for short chains are computationally fast and useful to obtain a general insight into the behaviour of the system. In the following section, the same procedure is repeated for long chains ($N = 100$) in order to calculate the free energy of the system.

Long chains

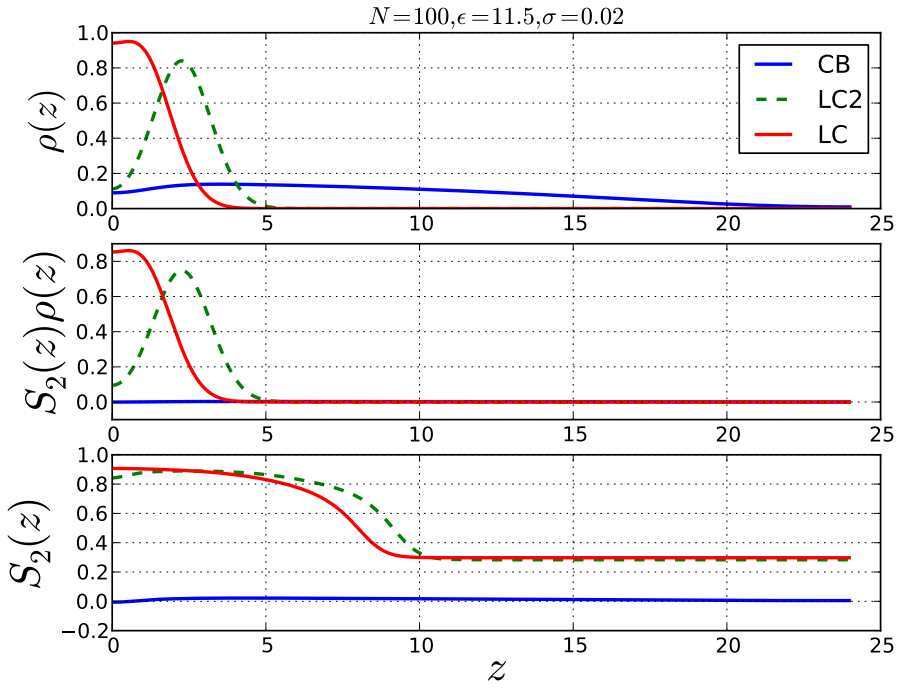

Figure 5.11: Three different configuration of polymer chains consisting of $N = 100$ rods. ϵ and σ are the LC coupling parameter and grafting density, respectively. Similar to the case of the short chains, the CB structure is a disordered phase extending throughout the system and the LC structure is a highly ordered dense brush collapsed near the wall. LC2 structure is also highly ordered with the same structure as the LC solution, but forming farther from the wall.

The equivalent solutions have been found for the long chains (Figure 5.11). The same procedure is used to find the free energies for the long chains (see Figure 5.12). By looking at the free energy diagram for long chains, the same behaviour as in short chains is observed. The only difference is that the free energy associated with the LC2 solution is closer to the LC free energy. The reason for this is that for longer chains, the structures of the LC and LC2 solutions are closer to each other and consequently the energy barrier is less between the two configurations. The important conclusion here is that the CB and LC phases are stable.

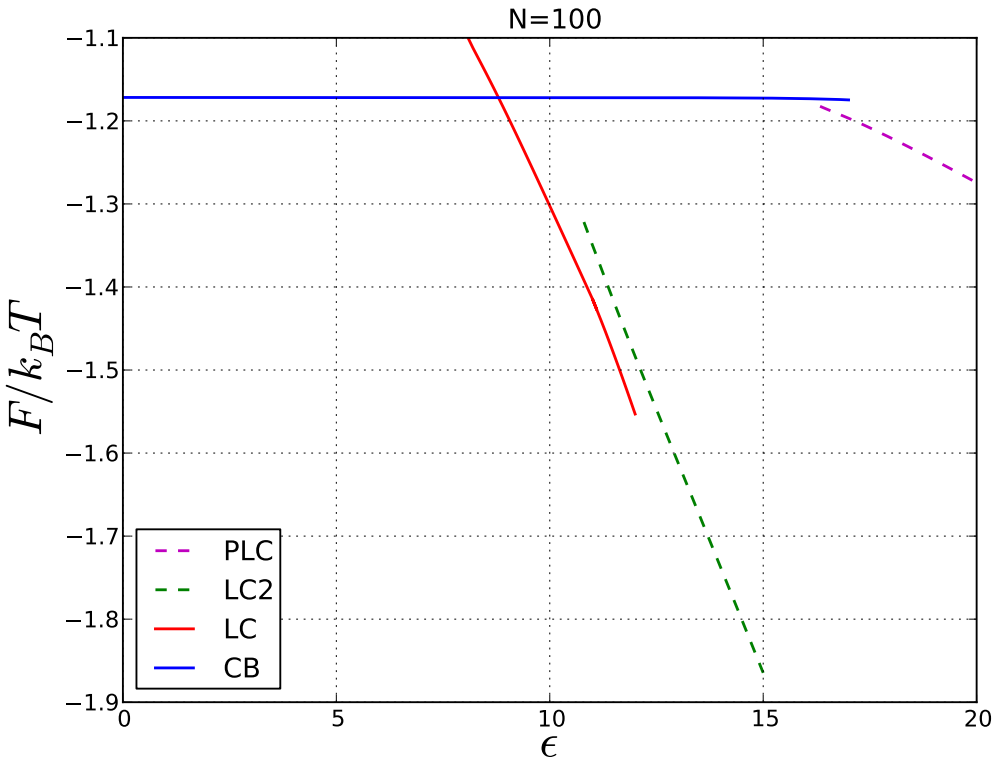

Figure 5.12: Free energy associated with three solutions found for brushes of long chains, $N = 100$ versus the anisotropic coupling parameter, ϵ. Similar to the case of short chains, for low ϵ values, the CB structure is stable and for high ϵ values, the LC phase is the stable solution. The LC2 structure is also unstable throughout the system. Also, it can be seen that for high ϵ, another unstable solution can be found (called PLC).

Additionally, Figure 5.12 shows that for high ϵ, an unstable solution can be found, which was not found for short chains. We call this solution a planar liquid crystalline (PLC) brush. Although this solution is unstable, it is interesting to look into its configuration. Figure 5.13 represents this structure. While the concentration profile looks similar to the LC results, the order parameter is close to $-\frac{1}{2}$. $S_2(z) = -\frac{1}{2}$ is indicative of a system in which molecules order parallel to the wall. This is a highly non-physical case because if all the molecules orient parallel to the wall, they would choose a new director within the x-y plane and then the S_2 would be found to be 1.0.

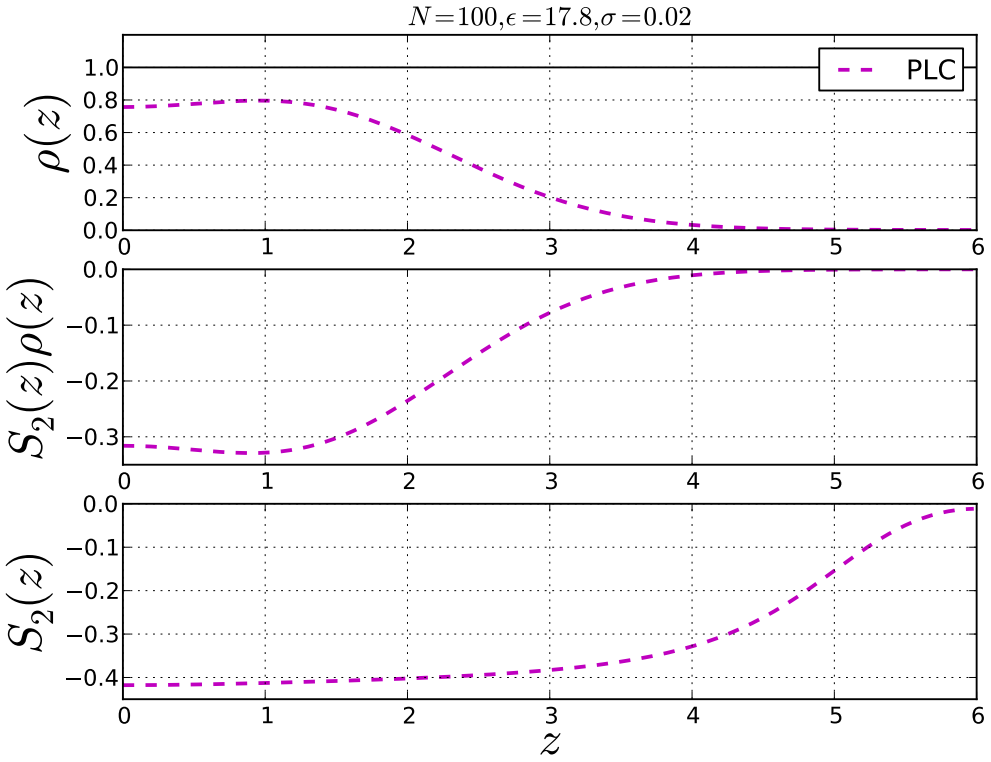

Figure 5.13: Polymer chain consisting of $N = 100$ freely-jointed rods with planar liquid crystalline (PLC) structure. ϵ and σ are the LC coupling parameter and grafting density, respectively. In the PLC state, similar to the LC phase, there is a dense concentration profile near the wall. However, $S_2(z)$ is close to $-\frac{1}{2}$ in contrast to $S_2(z) = 1$ that exists in the LC state. $S_2(z) = -\frac{1}{2}$ corresponds to a system where rods orient parallel to the wall, which is a highly non-physical case.

Figure 5.13 also shows that the order parameter increases from $-\frac{1}{2}$ to 0 far from the substrate ($z > 4$), while the concentration is very low (close to zero) in this region. In fact, any monomer located at $z > 4$ are from stretched chains and thus no longer parallel to the wall. As a result, $S_2(z)$ profile begins to increase far from the substrate.

This unstable phase (PLC) along with the two other phases (CB and LC) are also found in previous studies [20]. These results are shown in Figure 5.14.

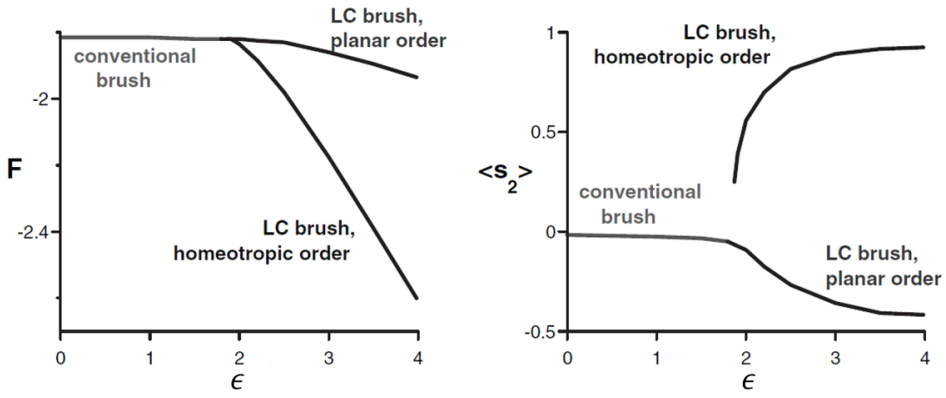

Figure 5.14: Free energy and order parameter found in the lattice model of Birshtein et al. [20]. The free energy diagram shows that for low ϵ values, the CB phase is stable while for high ϵ the homeotropic LC phase (perpendicular to the wall) has a lower free energy. Planar liquid crystalline phase is also found to be an unstable state. The order parameter diagram indicates that the LC phase (homeotropic) is highly ordered, $S_2(z) \approx 1$, and the CB phase is highly disordered with $S_2(z) \approx 0$. The degree of order for planar LC phase is also found to be $S_2(z) \approx -\frac{1}{2}$.

Our results agree with previously found configurations illustrated in Chapter 2. By comparing Figure 5.15(a) with 5.16 , we see that our LC concentration profile is less sharp than previously found structures. This is because in the mentioned work, calculations are done on a lattice with only 6 choices of angle for the molecule's orientation, whereas in the current project, mesogenic units are able to freely orient. For the same reasons, there is a difference in the order parameter profile in Figures 5.15(b) with 5.16. Our results show a high degree of orientational order for LC structure next to the wall. However, as can be seen in Figure 5.15(b), the order parameter for LC structure is relatively small close to the wall and following that there is a sharp increase to $S_2(z) \approx 1$.

Apart from the LC and CB solutions, the Birshtein group [20] found a third solution with a configuration between the LC and CB ones [19], which they called a micro-segregated brush (MSB). It is reported that MSB is stable near the transition point of the LC and CB phase. However, our model could not predict this phase near the transition points. We have only found the LC and CB structures to be stable and there is no evidence of a third stable solution near the transition point.

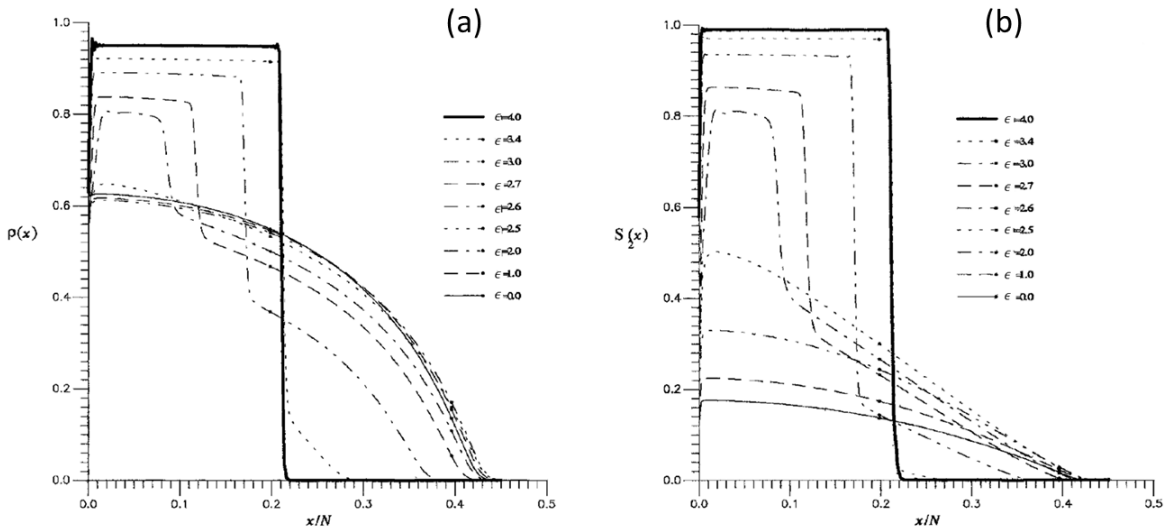

Figure 5.15: (a) Concentration profiles for different values of anisotropic coupling parameter, ϵ, from the lattice model of Birshtein et al. [20]. For weak LC interactions (low ϵ), the brush exhibits the conventional parabolic-like profile (CB phase), while for strong LC interactions (high ϵ), the polymers crystallize into a dense brush with a step-like profile (LC phase). At intermediate interaction strengths, a phase is found in which the brush exhibits a crystalline layer next to the grafting surface with an external layer similar to the conventional brush. They called this state a micro-segregated brush (MSB) phase. The LC concentration profile is sharp compared to our results since their calculations are done on a lattice with only 6 choices of configuration. (b) The degree of orientational order profile for different values of anisotropic coupling parameter, ϵ, from the lattice model of Birshtein et al. [20]. By increasing the anisotropic coupling parameter, ϵ, the order parameter increases from the CB phase to the LC phase, where $S_2(z) = 1$ and it is highly ordered. Since their calculations are done on a lattice with only 6 choices of configuration, the degree of order found for LC phase next to the wall is lower than our results.

In conclusion, our study showed that only two stable phases exist; CB that forms at low ϵ and LC, which occurs at high ϵ. A first order transition occurs between these two phases, since there is a sharp transition in the free energy diagram (the first derivative of the free energy is discontinuous).

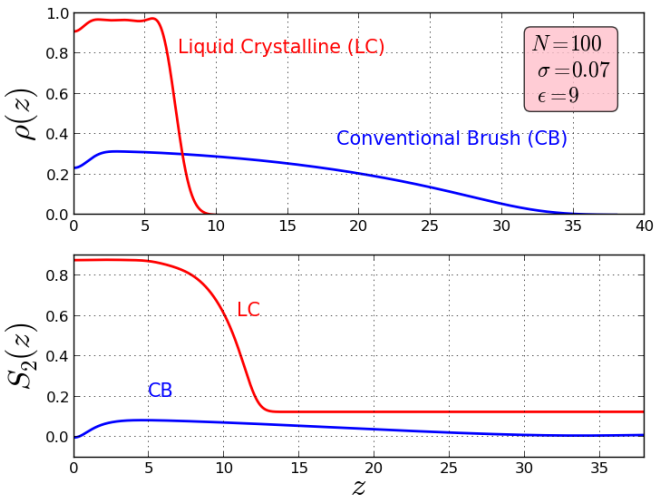

Figure 5.16: Stable configurations of polymer chains with $N = 100$ freely-jointed rods and grafting density of $\sigma = 0.07$ with the LC coupling parameter of $\epsilon = 9$.

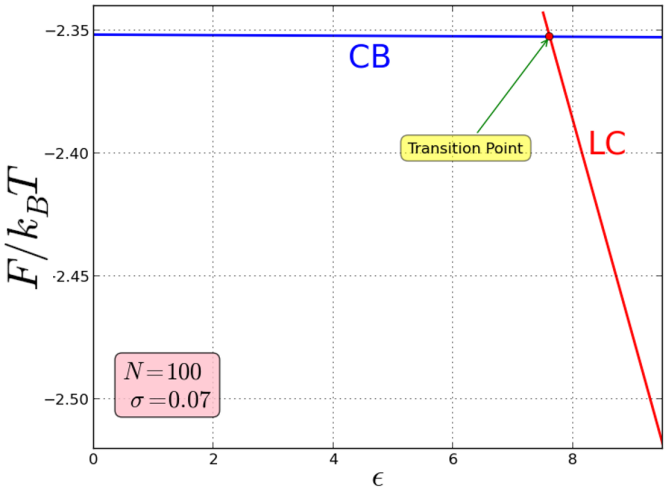

Figure 5.17: Free energy associated with the LC and the CB phase. There is a first order transition between these two phases. For the parameters shown in Figure 5.16 the LC phase is stable.

So far, the free energy of the system has been calculated for different ϵ. Grafting density is another variable that affects the behaviour. Thus, we need to investigate the free energy for different grafting densities. In Figure 5.18, the free energy is calculated for a range of ϵ values and the transition points are determined for a number of different grafting densities. It can be concluded from the diagram that for sparsely grafted chains, the transition occurs at much higher ϵ compared to highly dense chains. In fact, low grafting densities result in lower interaction between the chains. Thus, a stronger anisotropic field is required to generate the LC phase.

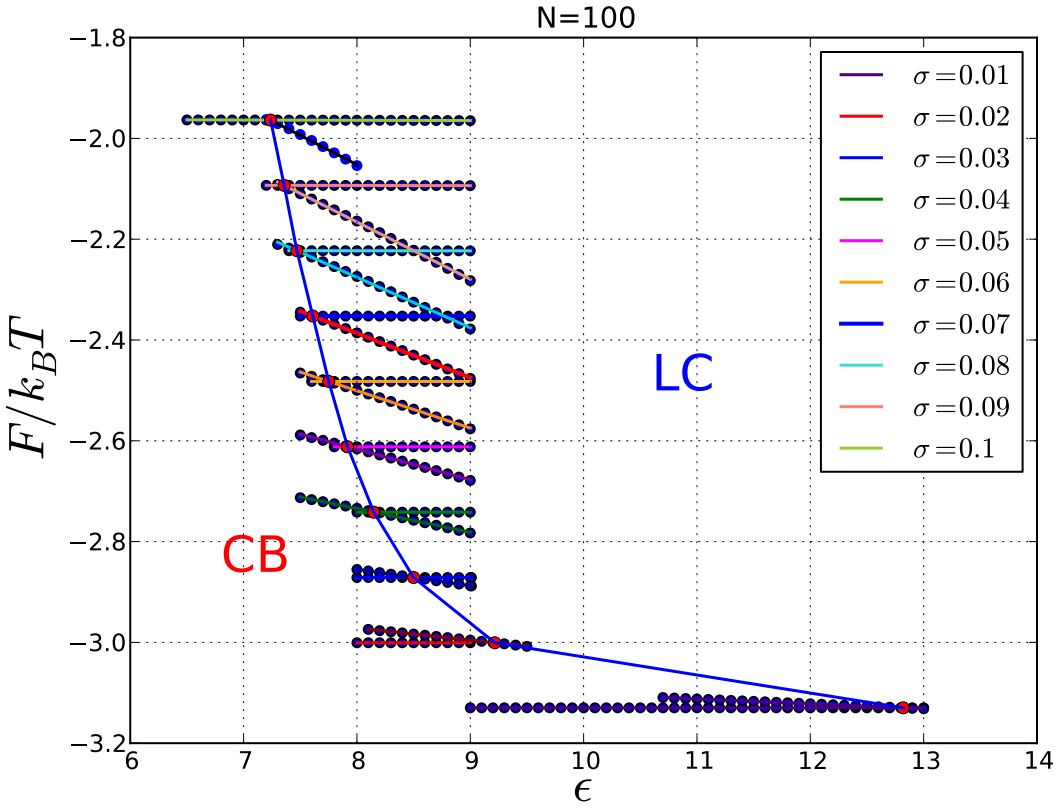

Figure 5.18: Free energy versus the LC coupling parameter, ϵ, for a number of different grafting densities, σ, of polymer chains consisting of $N = 100$ freely-jointed rods. At each σ, the free energy associated with the CB and the LC phase is calculated and the transition points are connected to one another.

The phase transitions in Figure 5.18 are used to create a phase diagram. This is done for three different chain lengths. The phase diagram indicates that for high grafting densities, the transition points are very close for different chains lengths. In contrast, for sparsely grafted chains, the transition happens at very different values of ϵ. In fact, at low grafting densities, it is more difficult to force the chains to order due to small interactions between molecules. This becomes even more difficult when the chains are short. Thus, a higher ϵ is needed to generate the LC phase. This is evidently manifested in Figure 5.19.

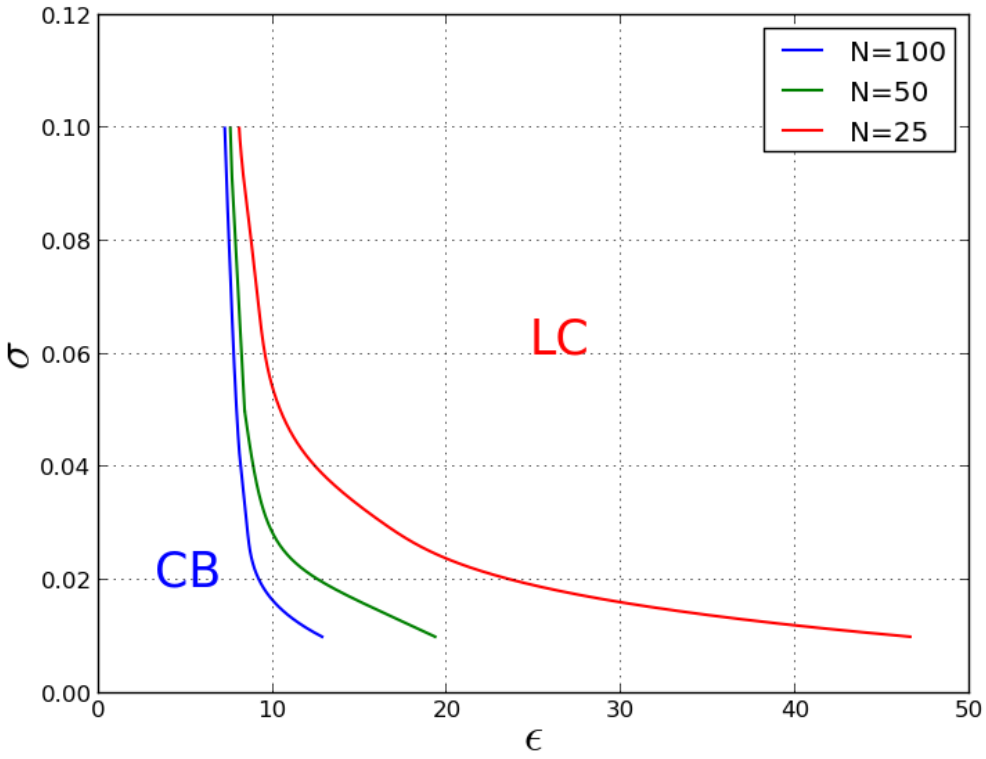

Figure 5.19: Phase diagram. The grafting density, σ, versus the anisotropic coupling parameter, ϵ, for polymer chains consisting of N freely-jointed rods. At high values of ϵ, the liquid crystalline phase is stable while the stable phase at low ϵ is the conventional brush. The figure shows that the transition points for three different chain lengths (25, 50, 100), are very close to each other at high grafting densities. However, transitions happen at very different ϵ for sparsely grafted chains. When grafting density is low, small interactions exist between the chains. Thus, a strong field is required (high ϵ) to order the chains.

Additionally, Figure 5.19 shows that by doubling N, results have been roughly doubled. Such relation suggests the possibility of defining the system by only two parameters ϵ and $N\sigma$. Figure 5.20 demonstrates a collapse in $N\sigma$ versus ϵ diagram, which indicates that this 3-parameter model is scaled to a system with 2 parameters. It can be a topic of future work to understand the theoretical explanation of this relation.

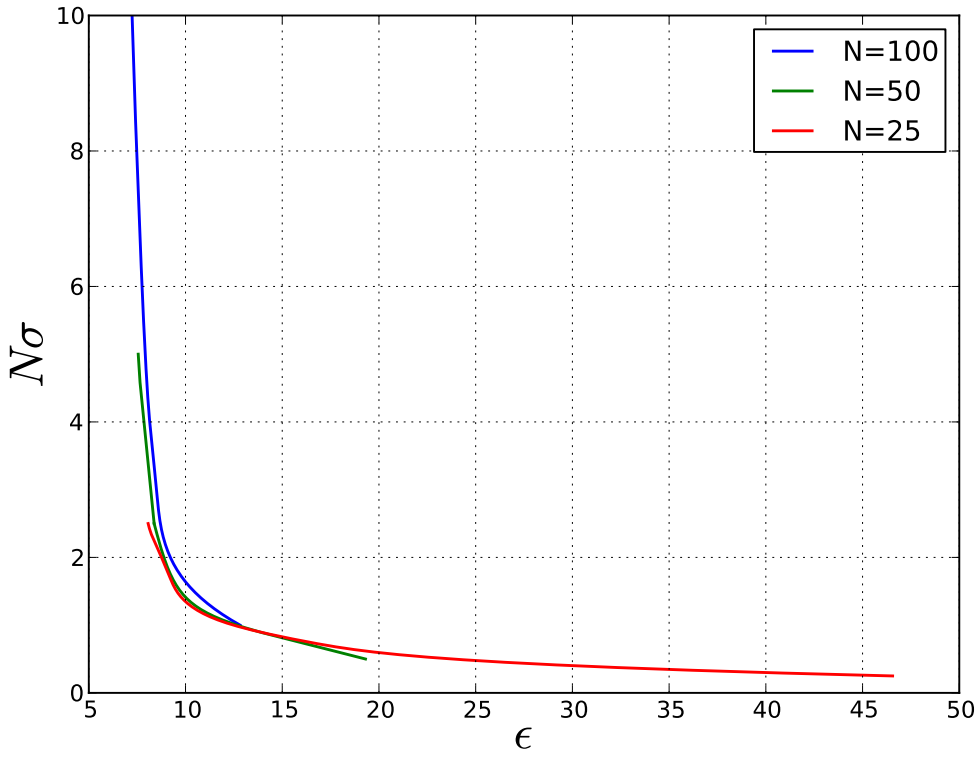

Figure 5.20: $N\sigma$ versus ϵ, for three different number of rods, N. σ is the grafting density and ϵ is the anisotropic coupling parameter. A collapse between the results suggest that the phase diagram can be generated by only two parameters ($N\sigma$ and ϵ).

Chapter 6

Conclusions and future work

We have derived a field-theoretic model to describe isotropic and anisotropic interactions in a system of liquid crystalline polymer brushes. Our model is considerably more realistic than previous models since it is an off-lattice model, in which polymer segments can freely orient. In summary, our results showed that:

- In the presence of a strong liquid crystalline field, the brush is collapsed near the wall and rigid parts lied in a zigzag manner. At this configuration, the degree of orientational order has a very high value demonstrating a well-ordered system.
- In the case of weak anisotropic interactions between the mesogens, a configuration similar to the structure of chains without any liquid crystalline segments is observed. In this case, system is highly disordered.
- The free energy associated with each solution has been found and stable structures have been identified. It is shown that a first-order transition exists between the conventional brush phase and the liquid-crystalline phase.
- A phase diagram is also created for this system, which indicates the effect of each parameter (grafting density, anisotropic coupling parameter and chain length) on the transition from one phase to another. It is shown that for high grafting densities, regardless of the chain size, smaller ϵ is required to form the LC phase. However, for low grafting densities, the phase transition depends on the chain length. Longer chains arrange in the LC phase easier than shorter ones. Thus, the transition happens at smaller ϵ.

6.1 Future work

The current project provides a basis for more research to improve the described model of LC polymer brushes. The model can be further developed as follows:

- A liquid crystalline polymer brush consists of rigid segments connected with flexible connectors. Thus, they are in the category of semi-flexible polymers. So far, no constraint has been placed on the flexibility of chains and they could easily fold back and forth. In order to improve the model, a bending energy should be included to control the stiffness and flexibility of the chains. This makes the model more realistic since LC polymers are not completely freely jointed.

- It has been explained in the theory section that average isotropic interactions of polymer and solvent molecules are represented by average fields as follows:

$$w_p(z) = \chi \int f(z - z')\rho_s(z')dz' + \xi(z)$$
$$w_s(z) = \chi \int f(z - z')\rho_p(z')dz' + \xi(z)$$

  In this project, we have studied athermal solvents where $\chi = 0$. Thus, in the above equations, only one term would remain, which is the pressure field enforcing the incompressibility condition. However, one can extend this study by investigating the system under different values of χ.

- The current project investigated the phase behaviour of LC polymer brushes immersed in a non-liquid crystalline solvent. In order to reach a complete conclusion about the potential of this work toward the mentioned application in Chapter 1, i.e. alignment layers in LCDs, it is required to study this system with liquid crystalline solvents. It is interesting to understand the effect of LC polymer chains on their surrounding LC solvent molecules. This can also be done by employing self-consistent field theory and introducing a field to represent the anisotropic interactions between LC solvent molecules and LC polymer chains.

- The current model of LC polymer chains can be used to study the configuration and phase behaviour of two LC brushes placed face to face and immersed in a solvent, which has been done with the lattice model [18]. Our model can easily be extended to include two polymer chains by mirroring the boundary conditions.

Appendix A

Bond energy for rigid rods

In this Appendix, our aim is to show

$$\frac{1}{4\pi a^2}\int\int \delta(|\mathbf{r}|-a)dxdy = \begin{cases}(2a)^{-1}, & \text{if } |z|<a \\ 0, & \text{if}\,|z|>a\end{cases} \tag{A.1}$$

By switching to cylindrical coordinates we have

$$\int \delta(|\mathbf{r}|-a)dxdydz = \int \delta(|\mathbf{r}|-a)\rho d\rho d\phi dz \tag{A.2}$$

Thus,

$$\int \left[\int\int \delta(|\mathbf{r}|-a)\rho d\rho d\phi\right] dz = \int h(z)dz \tag{A.3}$$

We are looking to find $h(z)$

$$h(z) = \int\int \delta(|\mathbf{r}|-a)\rho d\rho d\phi = 2\pi\int \delta(|\mathbf{r}|-a)\rho d\rho \tag{A.4}$$

Since $r=\sqrt{\rho^2+z^2}$. we can rewrite the above equation as

$$h(z) = 2\pi\int_0^{\sqrt{a^2-z^2}} \delta(\sqrt{\rho^2+z^2}-a)\rho d\rho \tag{A.5}$$

Now, we can use one of the properties of Dirac delta function, that is

$$\delta(f(x)) = \frac{\delta(x - x_0)}{|f'(x)|} \tag{A.6}$$

which is valid if x_0 is a single root. Comparing the delta function in equation A.5 with above relation we find

$$\begin{aligned} f(\rho) &= \sqrt{\rho^2 + z^2} - a \\ \rho_0 &= \sqrt{a^2 - z^2} \\ f'(\rho) &= \frac{\rho}{\sqrt{\rho^2 + z^2}} \end{aligned} \tag{A.7}$$

So, equation A.5 changes to

$$h(z) = 2\pi \int_0^{\sqrt{a^2-z^2}} \delta(\rho - \sqrt{a^2 - z^2}) \rho \frac{a}{\sqrt{a^2 - z^2}} d\rho \tag{A.8}$$

Here we can make use of another property of Dirac delta function, which is

$$\int \delta(x - x_0) f(x) dx = f(x_0) \tag{A.9}$$

Thus, when $|z| < a$ we have

$$h(z) = 2\pi\sqrt{a^2 - z^2} \frac{a}{\sqrt{a^2 - z^2}} = 2\pi a \tag{A.10}$$

The integral in equation A.1 results in $2\pi a$ in the constrain of $|z| < a$. Multiplying the pre-factor $\frac{1}{4\pi a^2}$ would prove the answer in equation A.1.

References

[1] M.W. Matsen , Self-consistent field theory and its applications, Soft Matter 1 (2006): 87-178.

[2] Brittain, William J., and Sergiy Minko. Structural definition of polymer brushes. Journal of Polymer Science Part A: Polymer Chemistry 45.16 (2007): 3505-3512.

[3] Advincula, Rigoberto C. Polymer Brushes: Synthesis, Characterization, Applications. Weinheim: Wiley-VCH, 2004.

[4] Peng, Bin. Liquid crystal polymer brushes and their application as alignment layers in liquid crystal cells. Diss. Ph. D. thesis, Johannes Gutenberg-Universitt Mainz, 2000.

[5] Zdyrko, Bogdan, and Igor Luzinov. Polymer brushes by the "grafting to method. Macromolecular rapid communications 32.12 (2011): 859-869.

[6] Sergiy Minko. Grafting on Solid Surfaces: "Grafting to and "Grafting from Methods. Springer Berlin Heidelberg (2008) 215-234

[7] Collings, Peter J., and Michael Hird. Introduction to Liquid Crystals: Chemistry and Physics. London: Taylor Francis, 1997.

[8] Image by Kebes (Own work) [CC BY-SA 3.0 (http://creativecommons.org/licenses/by-sa/3.0)

[9] Image by Kebes (Own work) [CC BY-SA 3.0 (http://creativecommons.org/licenses/by-sa/3.0)

[10] Kleman, Maurice, and Oleg D. Lavrentovich. Soft Matter Physics: An Introduction. New York: Springer, 2003.

[11] Wang, Xinjiu, and Qifeng Zhou. Liquid Crystalline Polymers. Singapore: World Scientific Pub., 2004.

[12] Ciferri, Alberto. Liquid Crystallinity in Polymers: Principles and Fundamental Properties. New York: VCH, n.d.

[13] Donald, A. M., A. H. Windle, and S. Hanna. Liquid Crystalline Polymers. Cambridge: Cambridge UP, 1992.

[14] Hoogboom, Johan, Theo Rasing, Alan E. Rowan, and Roeland J. M. Nolte. "LCD Alignment Layers. Controlling Nematic Domain Properties." J. Mater. Chem. 16.14 (2006): 1305-314.

[15] Halperin, A., and D. R. M Williams. "Liquid Crystalline Brushes: An Anchoring Transition." Europhysics Letters (EPL) Europhys. Lett. 21.5 (1993): 575-80.

[16] Halperin, A., and D. R M Williams. "Liquid Crystalline Polymers in Nematic Solvents: Interfacial Behaviour and Active Anchoring." Journal of Physics: Condensed Matter J. Phys.: Condens. Matter 6.23A (1994): n. pag

[17] Deng, Mingge, et al. "Wormlike polymer brush: a self-consistent field treatment." Macromolecules 43.7 (2010): 3455-3464.

[18] Amoskov, Victor M., Tatiana M. Birshtein, and Victor A. Pryamitsyn. "Theory of Liquid-Crystalline (LC) Polymer Brushes: Interpenetrating Brushes." Macromolecules 31.11 (1998): 3720-730.

[19] Amoskov, Victor M., Tatiana M. Birshtein, and Victor A. Pryamitsyn. "Theory of Polymer Brushes of Liquid-Crystalline Polymers." Macromolecules 29.22 (1996): 7240-250.

[20] Mercurieva, Anna A., Tatiana M. Birshtein, and Victor M. Amoskov. "Theory of Liquid-crystalline Ordering in Polymer Brushes." Macromolecular Symposia Macromol. Symp. 252.1 (2007): 90-100.

[21] Kawakatsu, Toshihiro. Statistical Physics of Polymers: An Introduction. Berlin: Springer, 2004.

[22] Becker, Oren M. Computational Biochemistry and Biophysics. New York: M. Dekker, 2001.

[23] Fredrickson, Glenn Harold. The Equilibrium Theory of Inhomogeneous Polymers. Oxford: Clarendon, 2006.

[24] Solvation Models [PowerPoint slides]. Retrieved from http://chem.yu.edu.jo/rawash/chem%20495/Solvation%20Models.ppt

[25] Kim, J. U., and M. W. Matsen. "Finite-stretching Corrections to the Milner-Witten-Cates Theory for Polymer Brushes." The European Physical Journal E Eur. Phys. J. E 23.2 (2007): 135-44.

[26] Hamming, R. W. Numerical Methods for Scientists and Engineers. N.p.: n.p., n.d.

[27] Tzeremes, G., K. . Rasmussen, T. Lookman, and A. Saxena. "Efficient Computation of the Structural Phase Behavior of Block Copolymers." Physical Review E Phys. Rev. E 65.4 (2002): n. pag.

[28] Thompson, R. B., K. . Rasmussen, and T. Lookman. "Improved Convergence in Block Copolymer Self-consistent Field Theory by Anderson Mixing." The Journal of Chemical Physics J. Chem. Phys. 120.1 (2004): 31.

[29] Matsen, M. W. "Fast and Accurate SCFT Calculations for Periodic Block-copolymer Morphologies Using the Spectral Method with Anderson Mixing." The European Physical Journal E Eur. Phys. J. E 30.4 (2009): 361-69.

[30] Peng, B., J. Rhe, and D. Johannsmann. "Homogeneously Aligned Liquid-Crystal Polymer Brushes." Adv. Mater. Advanced Materials 12.11 (2000): 821-24.

[31] Vlasova, Elena, Boris Volchek, Irina Tarasenko, and Guennadii Vlasov. "Spectroscopic Investigation of Polypeptide Plane Brushes." Macromolecular Symposia Macromol. Symp. 305.1 (2011): 116-21.

[32] Peng, Bin, Diethelm Johannsmann, and Jrgen Rhe. "Polymer Brushes with Liquid Crystalline Side Chains." Macromolecules 32.20 (1999): 6759-766.

[33] Johannsmann, Diethelm, Bin Peng, and Jurgen Ruhe. Process for Producing a Polymeric Liquid Crystal Alignment Layer, Use of Such an Alignment Layer, and Liquid Crystal Display Comprising Such an Alignment Layer. Patent EP 1158349 A1. 15 May 2000.

[34] Gedde, U. W. Polymer Physics. London: Chapman & Hall, 1995.

[35] Amoskov, Victor M., Tatiana M. Birshtein, and Victor A. Pryamitsyn. "Theory of Liquid-Crystalline (LC) Polymer Brushes: Interpenetrating Brushes." Macromolecules 31.11 (1998): 3720-730.